NORTHERN TERRITORY GEOLOGICAL SURVEY

RECORD 2025-003

Summary of results. NTGS laser ablation ICP–MS zircon and rutile age constraints on the basement to the Limbunya Group in drillhole LBD2

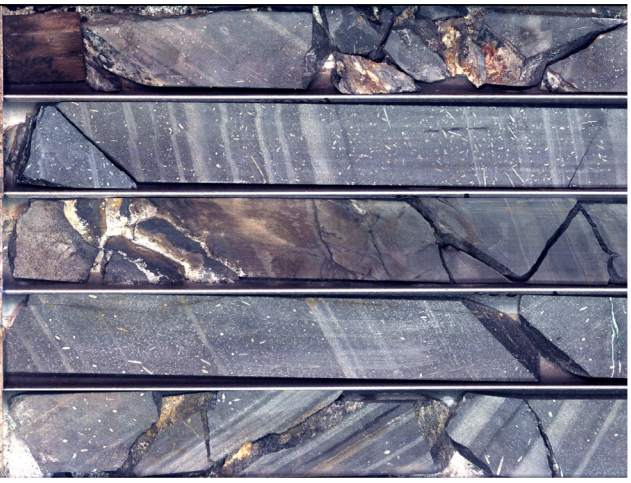

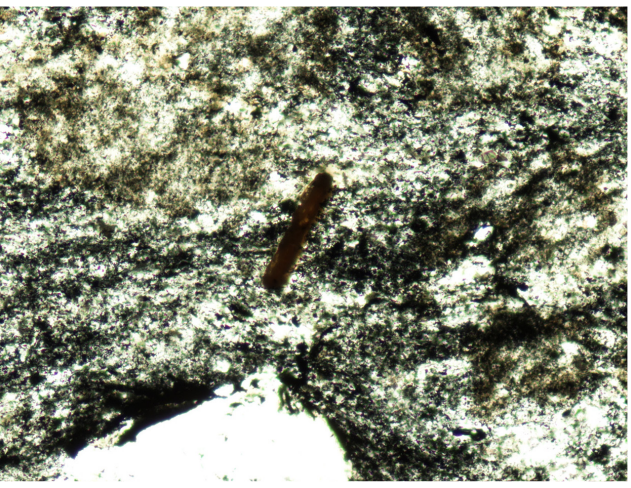

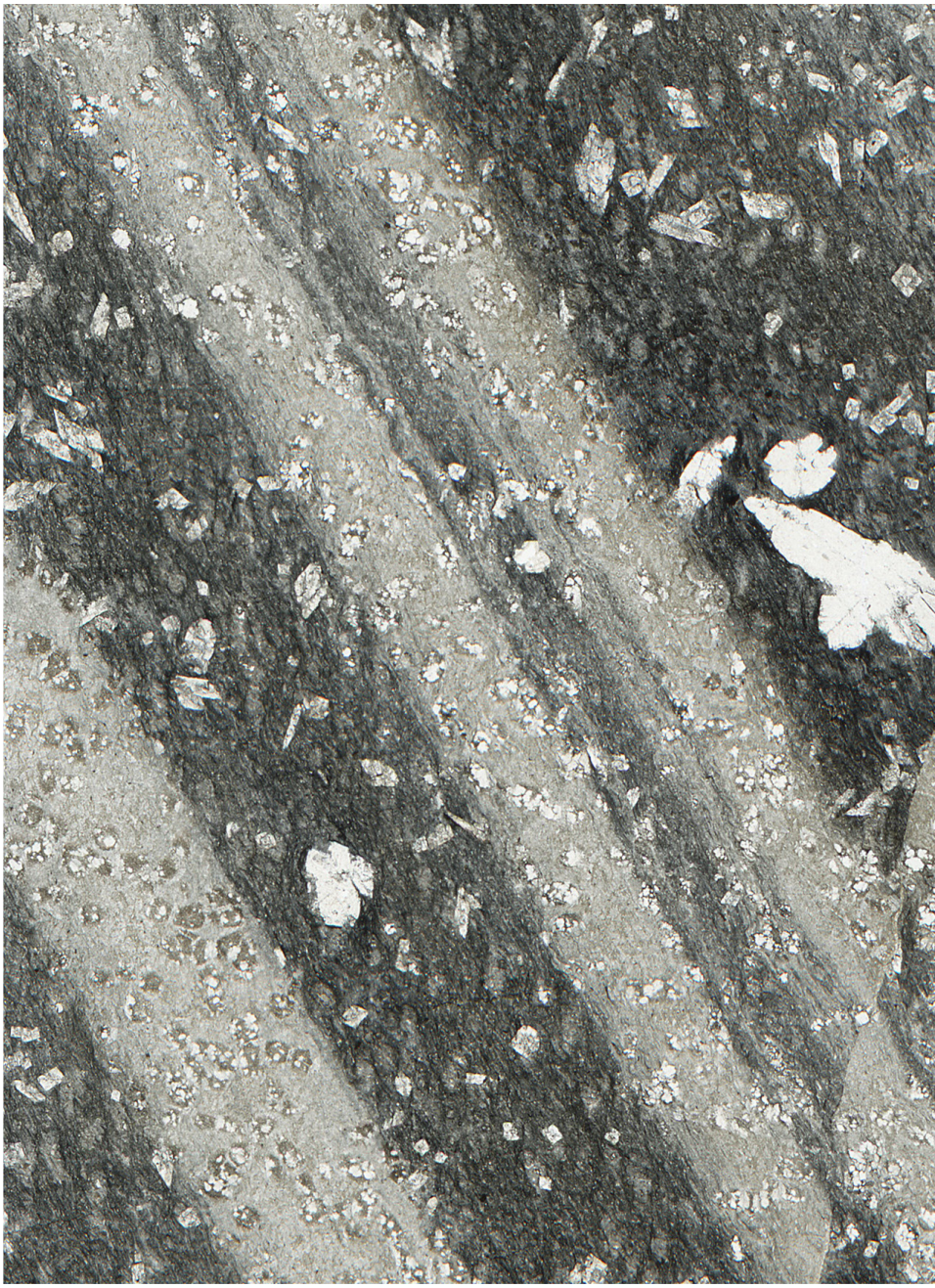

BL Reno, I Belousov and M Morissette

CODES
CENTRE FOR ORE DEPOSIT AND EARTH SCIENCES

NORTHERN TERRITORY GOVERNMENT

RESOURCING THE TERRITORY

DEPARTMENT OF MINING AND ENERGY
MINISTER: Hon. Gerard Maley, MLA
CHIEF EXECUTIVE OFFICER: Alister Trier

NORTHERN TERRITORY GEOLOGICAL SURVEY
SENIOR EXECUTIVE DIRECTOR: Ian Scrimgeour

BIBLIOGRAPHIC REFERENCE: Reno BL, Belousov I[1] and Morissette M[1], 2025. Summary of results. NTGS laser ablation ICP–MS zircon and rutile age constraints on the basement to the Limbunya Group in drillhole LBD2. *Northern Territory Geological Survey, Record* 2025-003.

(Record / Northern Territory Geological Survey ISSN 1443-1149)
ISBN: 978-0-7245-7434-6 (PDF)

Keywords: geochronology, Birrindudu Group, Limbunya Group, Birrindudu Basin, Ware Group, Tanami Group, Tanami Region, Woodcutters Supergroup, Pine Creek Orogen, LBD2, LA–ICP–MS, U–Pb, zircon, rutile.

Editor: S McLaren. Layout and graphics: KJ Johnston.

Northern Territory Geological Survey
3rd floor Paspalis Centrepoint Building
Smith Street Mall, Darwin
GPO Box 4550
Darwin NT 0801, Australia

Arid Zone Research Institute
South Stuart Highway, Alice Springs
PO Box 8760
Alice Springs NT 0871, Australia

For further information contact:
Minerals and Energy InfoCentre
Phone +61 8 8999 6443
Website: https://dme.nt.gov.au
https://resourcingtheterritory.nt.gov.au
Email: geoscience.info@nt.gov.au

[1] CODES, University of Tasmania, Hobart, TAS 7001, Australia

Summary of results. NTGS laser ablation ICP–MS zircon and rutile age constraints on the basement to the Limbunya Group in drillhole LBD2

by

BL Reno, I Belousov and M Morissette

SUMMARY

New laser ablation inductively-coupled plasma mass spectrometry (LA–ICP–MS) U–Pb geochronological data are reported for zircon and rutile from samples from two intervals of drillhole LBD2 beneath the Limbunya Group of the Birrindudu Basin, Northern Territory.

Sample LB23BLR001 is a metamudstone, from the depth interval 451.5–459.41 m, that has undergone amphibolite facies metamorphism. The sample preserves evidence for two phases of metamorphism: an early graphite–cordierite–rutile assemblage that defines a pervasive weak grain shape foliation; and a younger assemblage of randomly-oriented andalusite and rutile that overprints the graphite–cordierite fabric. Fabric development in this sample occurred ca 1.86–1.70 Ga, with a thermal overprint at approximately 1.62 Ga, and a later thermal, hydrothermal, or alteration event at 234 ± 34 Ma.

Sample LB23BLR002 is a metatuff or metamudstone from the depth interval 386.2–391.9 m that has been pervasively recrystallised. A rutile age of ca 2.06 Ga likely represents the timing of volcanism or deposition of the interval; it may alternatively represent the timing of pervasive recrystallisation and metamorphism in the sample. A younger age of ca 1.72 Ga records a metamorphic overprint.

The probable deposition age of ca 2.06 Ga or older indicates that basement to the Limbunya Group in LBD2 may not belong to any known lithostratigraphic unit in the Tanami Region. If the deposition age is ca 2.06 Ga, then the basement rocks may instead correlate to, or be coeval with, the Woodcutters Supergroup in the Pine Creek Orogen; if the ca 2.06 Ga age represents the timing of recrystallisation of the sample, then the interval would correlate to an older lithostratigraphic unit. Further study is required to confidently interpret the lithostratigraphic unit and geological province beneath the Birrindudu Basin in drillhole LBD2.

The analyses aim to identify the rocks, and to determine their age and the timing of any metamorphism or alteration they experienced, providing insights into the lithology and provenance of the rocks beneath the Birrindudu Basin.

CONTENTS

FIGURES

TABLES

APPENDICES

INTRODUCTION

This Record presents the results of the mineral isotopic geochronology analyses conducted at the ARC Centre of Excellence in Ore Deposits (CODES) at the University of Tasmania on samples from drillhole LBD2 (**Figure 1**). LBD2 intersects metasedimentary and metaigneous rocks beneath the Birrindudu Basin; these rocks have been hypothesised to belong to, or be coeval with, rocks of the Tanami Region or the Pine Creek Orogen but their

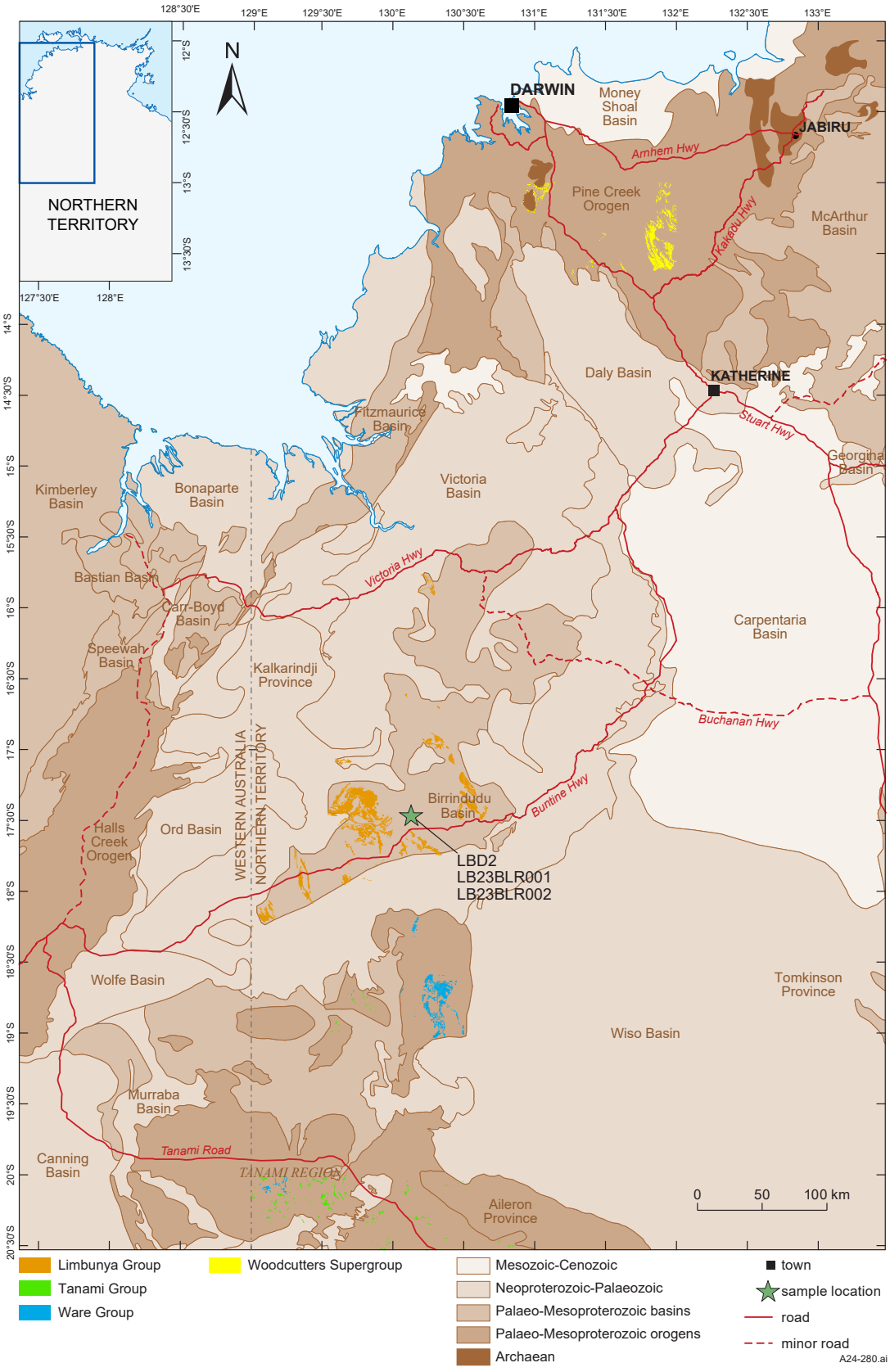

Figure 1. Regional geological map showing location of samples analysed. The outcrop extent of the lithostratigraphic groups and supergroups discussed in the text from the Northern Territory Geological Survey (2023). The Inverway Metamorphics are too small to depict at this scale but are located within the area mapped as Limbunya Group. Some road data is copyrighted OpenStreetMap and available from https://www.openstreetmap.org and https://opendatacommons.org.

lithology and provenance have remained unconstrained. Zircon and rutile were analysed in two metasedimentary samples to constrain the age and identity of the unknown basement rocks as well as the timing of any metamorphism or alteration they experienced.

This record documents the location, lithology, and geologic context of each sample; the petrologic context of the zircon and rutile in each sample; and the isotopic data collected from zircon and rutile in each sample. A chronologic interpretation is also provided for each sample. A summary of sample information and analytical results is provided in **Table 1**, with sample and grain imagery in **Appendix 1** and the full analytical results in **Appendix 2**.

Table 1. Summary of LA–ICP–MS samples and results. Sample coordinates are referenced to the Map Grid of Australia 1994 (MGA94), Zone 53. Uncertainties are given at the 95% confidence level.

Sample No.	Latitude	Longitude	Lithology	Age (Ma)	Interpretation
LB23BLR001	-17.46228	130.128319	metamudstone	1.86–1.70 Ga	pre-dates, or dates fabric development
LB23BLR001	-17.46228	130.128319	metamudstone	ca 1.62 Ga	thermal overprint
LB23BLR001	-17.46228	130.128319	metamudstone	234 ± 34 Ma	thermal overprint
LB23BLR002	-17.46228	130.128319	metatuff or metamudstone	ca 2.06 Ga	deposition
LB23BLR002	-17.46228	130.128319	metatuff or metamudstone	ca 1.72 Ga	metamorphism

Analytical procedures

All zircon and rutile U–Pb isotopic analyses presented in this report were undertaken by LA–ICP–MS at CODES Analytical Laboratories, University of Tasmania.

Sample preparation

Mineral separation commenced with ~200–400 g of rock crushed in a Cr-steel ring and milled to a grain size <4000 micron. Heavy minerals were separated using a gold pan, and magnetic minerals were removed by a Fe–B–Nd hand magnet. The heavy mineral portion was placed on double-sided tape, and epoxy glue was then poured to form a 2.5 cm diameter disc mount. The mount samples were dried for 12 hours, polished using clean sandpaper and polishing lap, and then washed in distilled water in an ultrasonic bath.

Zircon and rutile location and imaging

The Mineral Liberation Analyser (MLA) at the Central Science Laboratory (CSL) of the University of Tasmania (**Appendix 1**) was used to create a full backscattered electron (BSE) image of each grain mount. Individual zircon and rutile grains were identified using a combination of relative BSE intensity and subsequent x-ray analysis.

Zircon and rutile searches were performed on polished grain mounts coated with 20 nm of carbon using a FEI MLA 650 tungsten-filament scanning electron microscope (SEM) equipped with a Bruker Quantax Esprit 2.1 EDS system with two XFlash 5030 SDD detectors. BSE images and energy dispersive x-ray spectra for MLA were collected using an accelerating voltage of 20 keV, a total x-ray intensity ~600 000 cps, and a dead time of ~32% (on quartz). BSE contrast and brightness were adjusted on silver and epoxy. A resolution of 512 × 512 pixels was used at 194× magnification resulting in a pixel size of 3 × 3 μm^2. The Bruker AMICS software version 3 and the particle method were used to discriminate mineralogy in the samples.

After classification and identification of zircon, cathodoluminescence (CL) imagery was collected for individual grains on the same SEM using a Gatan PanaCL-F CL detector at 10 kV accelerating voltage.

Isotope analysis

Trace element and U–Pb analyses were performed on zircon and rutile using an Agilent 7900 quadrupole inductively coupled plasma mass spectrometer (ICP–MS), coupled with a 193 nm Coherent Ar-F excimer laser equipped with the Resonetics S155 ablation cell (**Table 2**).

Each analysis began with a 30-second blank gas measurement followed by a further 30-second analysis time once the laser was switched on. Rutile was ablated using 20 µm spots at 5 Hz and an energy density of ~5 J/cm^2. Zircon was ablated using 20 µm spots at 5 Hz and an energy density of ~2.1 J/cm^2. A flow of He carrier gas at a rate of 0.35 l/min carried particles ablated by the laser out from the chamber to be mixed with Ar gas and carried to the plasma torch. Approximately 2 ml of nitrogen was also added to increase sensitivity at heavier masses.

For rutile, isotopes measured were ^{24}Mg, ^{27}Al, ^{29}Si, ^{43}Ca, ^{49}Ti, ^{55}Mn, ^{57}Fe, ^{89}Y, ^{90}Zr, ^{93}Nb, ^{118}Sn, ^{140}Ce, ^{146}Nd, ^{147}Sm, ^{153}Eu, ^{157}Gd, ^{163}Dy, ^{166}Er, ^{172}Yb, ^{178}Hf, ^{181}Ta, ^{182}W, ^{202}Hg, ^{204}Pb, ^{206}Pb, ^{207}Pb, ^{208}Pb, ^{232}Th, ^{235}U and ^{238}U with each isotope measured every ~0.23 seconds with longer counting time on the Pb and U isotopes compared to the other elements.

Data reduction, based on the method outlined in detail in Thompson *et al* (2016) and based on Chew *et al* (2014), involved a common Pb correction on the calibration standard. Intervals on the laser spectrum were chosen based on the lowest common Pb content and to avoid other mineral phases. For Pb/U ratios, downhole fractionation, instrument drift and mass bias correction factors were calculated using long-term average analyses of TB1 rutile (Thompson *et al* 2021, Jenkins *et al* 2023). For $^{207}Pb/^{206}Pb$ ratios (ages) instrument drift and mass bias correction factors were calculated using analyses of NIST610 glass and the Pb isotopic values of Baker *et al* (2004). Calibration of U–Pb ages was checked using several rutile reference materials that were treated as unknowns: R10 rutile (Luvizotto *et al* 2009) and R19 rutile (Zack *et al* 2011).

For zircon, isotopes measured were ^{31}P, ^{49}Ti, ^{56}Fe, ^{89}Y, ^{91}Zr, ^{93}Nb, ^{139}La, ^{140}Ce, ^{141}Pr, ^{146}Nd, ^{147}Sm, ^{153}Eu, ^{157}Gd, ^{159}Tb, ^{163}Dy, ^{165}Ho, ^{166}Er, ^{169}Tm, ^{172}Yb, ^{175}Lu, ^{178}Hf, ^{181}Ta, ^{204}Pb, ^{206}Pb, ^{207}Pb, ^{208}Pb, ^{232}Th, ^{235}U and ^{238}U with each element being measured every 0.25 seconds with longer counting

Table 2. LA–ICP–MS operating and data acquisition parameters.

Laser system	Coherent Ar-F gas laser
Laser wavelength	193 nm
Laser mode	Spot analysis
Nominal pulse width	c 20 ns
Repetition rate	5 Hz
Spot size (diameter)	20 µm
Fluence	2.1 (zircon), 5 (ruitle) J/cm^2
Ablation cell	Resonetics S155
Ablation cell gas flow rate (He)	0.35 l/min
Tubing for gas flow	Nylon 6
Laser beam focus	Fixed at sample surface
ICP–MS	Agilent 7900 quadrupole ICP–MS
Interface cones	cones for X lenses
Detector type	Dual mode Electron Multiplier
Detector mode	pulse counting for signals < 3.5 Mcps (Pb and U isotopes)
Detector vacuum	1.00E-05 Pa
Argon gas flow rate (l/min)	l/min
Plasma	14 l/min
Auxiliary	0.8 l/min
Sample	1.05 l/min
RF Power	1350 W
Lenses (V)	
Extract 1	2.4 V
Extract 2	-102 V
Data acquisition and processing	
Samples per peak	1
Acquisition mode	peak jumping
Integration type	counts per second
Mass resolution	300
Oxide production rate	<0.1 % ThO/Th
Analysis duration	c 90 s
Blank	30 s
Ablation	30 s
Washout	21 s

time on the Pb isotopes compared to the other elements. For each analysis, a subset of the data most closely matching a concordant composition was selected for quantification. For Pb/U ratios, downhole fractionation, instrument drift and mass bias correction factors were calculated using analyses of the 91500 zircon using values of Wiedenbeck *et al* (1995). For $^{207}Pb/^{206}Pb$ ratios and $^{207}Pb/^{206}Pb$ -based ages, instrument drift and mass bias correction factors were calculated using analyses of the NIST610 glass and the Pb isotopic values of Baker *et al* (2004). The calibration of the U–Pb ages was checked on analyses of Temora zircon (Black *et al* 2004) and Plešovice zircon (Sláma *et al* 2008) throughout the analytical session; these standards were treated as unknowns.

Trace element abundances in zircon and rutile were calibrated on NIST610 glass using values of Jochum *et al* (2011) and secondary standard corrections based on the compositions of glasses BCR-2G and GSD-1G (GeoReM preferred values; http://georem.mpch-mainz.gwdg.de/). Quantification was performed using ^{91}Zr as the internal standard element for zircon and ^{49}Ti as the internal standard element for rutile, normalizing all measured cations to 100% total oxide, assuming stoichiometric proportions. LADR software (Norris and Danyushevsky 2018) was used for data reduction. The primary and secondary standards, as well as NIST610, BCR-2G and GSD-1G glasses, were analysed in duplicate at the beginning, end, and every 60 minutes throughout the analytical session.

Standard and reference material data are included in **Appendix 2** and summarised in **Table 3**. Primary and secondary analyses are depicted in **Figure 2** for rutile and **Figure 3** for zircon.

Table 3. The preferred age of monazite reference standards used in this Record, and the geochronological results for the reference standards used in this Record.

Reference material	Phase	Reference	Reference method and isotope system	Preferred age	±2σ	This Record (same system)	±2σ
TB-1	rutile	Thompson *et al* 2021; Jenkins *et al* 2023	LA–ICP–MS Concordia	512.6	3.0	510	4
R10	rutile	Luvizotto *et al* 2009	ID-TIMS $^{206}Pb/^{238}U$	1091.6	3.5	1072	17
R19	rutile	Zack *et al* 2011	ID-TIMS Concordia	489.5	0.9	467	8
91500	zircon	Wiedenbeck *et al* 1995	ID-TIMS $^{206}Pb/^{238}U$	1062.4	0.4	1065	3
Temora	zircon	Black *et al* 2003	ID-TIMS Concordia	416.81	0.22	418	2
Plesovice	zircon	Slama *et al* (2008)	ID-TIMS Concordia	337.1	0.37	339	1

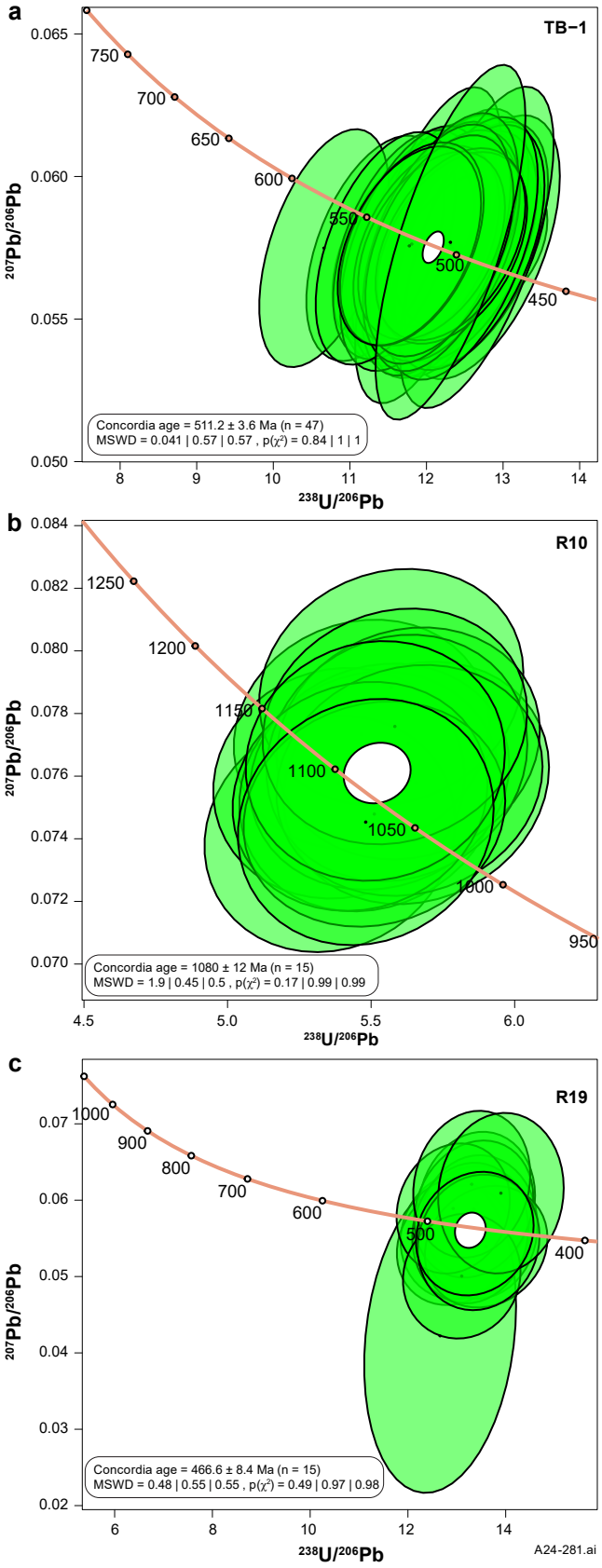

Figure 2. Tera-Wasserburg concordia diagram and weighted mean average plots for primary standards and reference rutile analysed in this study. The isotope system displayed in the weighted mean averages is the same as in the preferred age presented in **Table 2**. In concordia plots, the black dots show individual isotope analyses, green ellipses show 2σ confidence intervals, and the white ellipse represents the concordia age for the sample. In weighted mean average plots, analyses indicated in green are included in the mean and the analyses indicated in cyan are excluded. (**a**) TB-1 rutile concordia, (**b**) R10 rutile $^{206}Pb/^{238}U$, and (**c**) R19 rutile concordia.

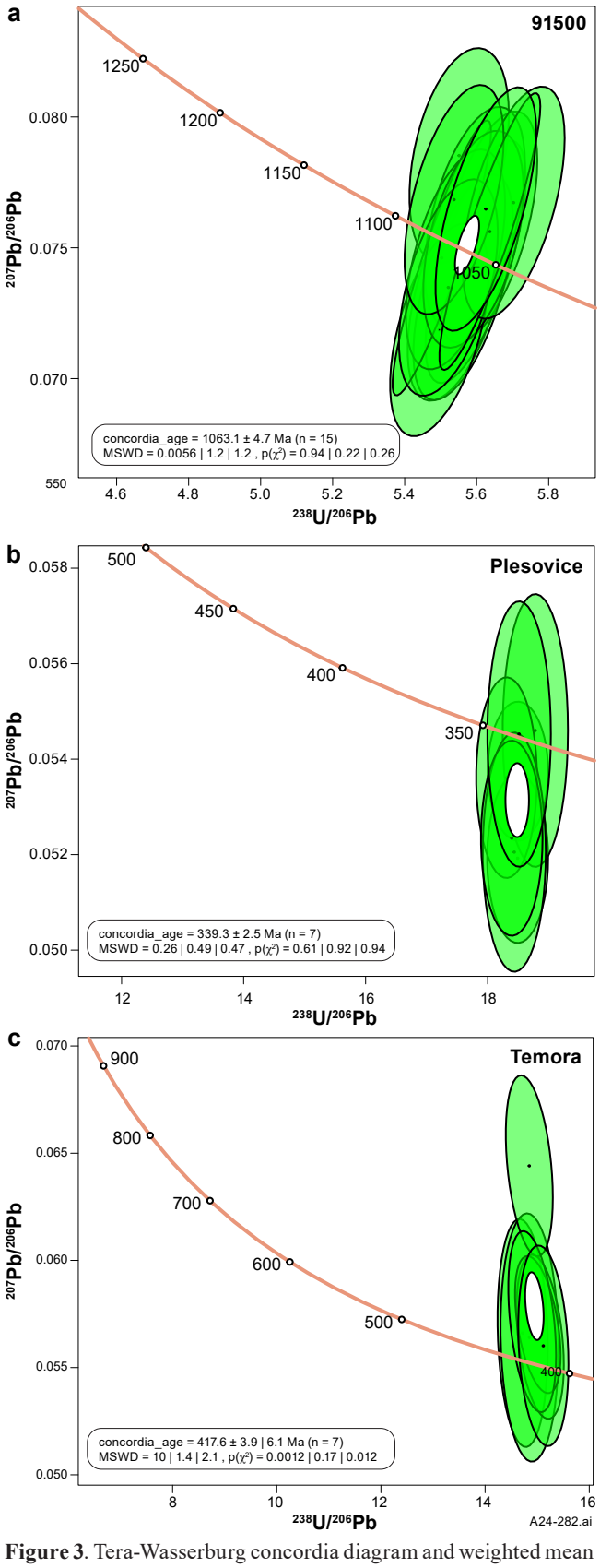

Figure 3. Tera-Wasserburg concordia diagram and weighted mean average plots for primary standards and reference zircon analysed in this study. The isotope system displayed in the weighted mean averages is the same as in the preferred age presented in **Table 2**. In concordia plots, the black dots show individual isotope analyses, green ellipses show 2σ confidence intervals, and the white ellipse represents the concordia age for the sample. In weighted mean average plots, analyses indicated in green are included in the mean and the analyses indicated in cyan are excluded. (**a**) 91500 zircon $^{206}Pb/^{238}U$, (**b**) Temora zircon concordia, and (**c**) Temora zircon concordia.

Data reduction and presentation

In this Record, an individual determination of time calculated from a single high-precision isotope analysis is referred to as a date; a normally distributed population of individual dates interpreted to record a single mineral growth or recrystallisation event is referred to as an age (Martin *et al* 2007, Baldwin and Brown 2008, Reno *et al* 2012, Schoene *et al* 2013). Unless stated otherwise, $^{207}Pb/^{206}Pb$ ages are quoted when discussing ages older than 1500 Ma; $^{206}Pb/^{238}U$ ages are quoted when discussing ages younger than 1500 Ma (see Spencer *et al* 2016).

Data, dates, and age interpretations were calculated and depicted using the packages IsoplotR 6.4 (Vermeesch 2018), ggplot2 (Wickham 2016), provenance (Vermeesch *et al* 2016), dplyr (Wickham *et al* 2023), tidyr (Wickham *et al* 2024), and viridis (Garnier *et al* 2024) in R 4.4.1 (R Core Team 2024) running in RStudio 2023.12.1+402 (Posit Team 2024). An R script containing the R code and data used for age calculations and production of all plots is included in **Appendix 1**; a subset of the relevant diagrams produced by that notebook is included as figures here.

No common lead corrections were made on the data in this record. Concordance and discordance were calculated using the formulae:

$$Concordance\ (\%) = 100 \times \frac{\left(\frac{^{206}Pb}{^{238}U}\right)_{date}}{\left(\frac{^{207}Pb}{^{206}Pb}\right)_{date}}$$

and

$$Discordance\ (\%) = 100\% - Concordance\ (\%)$$

Uncertainties on individual dates calculated from single isotope analyses are presented at a 1σ level; uncertainties on age calculations are presented at a 95% confidence level (see Vermeesch 2018 for details); and uncertainties on isotope and chemical data are presented at a 1σ level.

Assessment of concordance follows that of Spencer *et al* (2016) in that only analyses that fall along the 1:1 age line are within uncertainty of the concordia and therefore 'concordant'. Analyses that fall off this line cannot be considered concordant; radiogenic lead loss or some other isotopic disturbance cannot be discounted and must be considered in any age determination and interpretation.

Mineral abbreviations follow Siivola and Schmid (2007).

SAMPLES ANALYSED

Drillhole LBD2

Drillhole LBD2 (**Figure 4**), drilled in December 2009 to a depth of 751.6 m, targeted a magnetic and gravity anomaly within the Birrindudu Basin to assess the potential for Ni–Cu–PGE mineralisation related to rocks of the Kalkarindji Suite. Logging of the hole presented in Muir (2011) interpreted:

- 0–345.55 m: Limbunya Group of the Birrindudu Basin
- 345.55 m: unconformity
- 345.55–634.3 m: undivided Birrindudu Group of the Birrindudu Basin
- 634.3 m: unconformity
- 634.3–751.6 m: Inverway Metamorphics

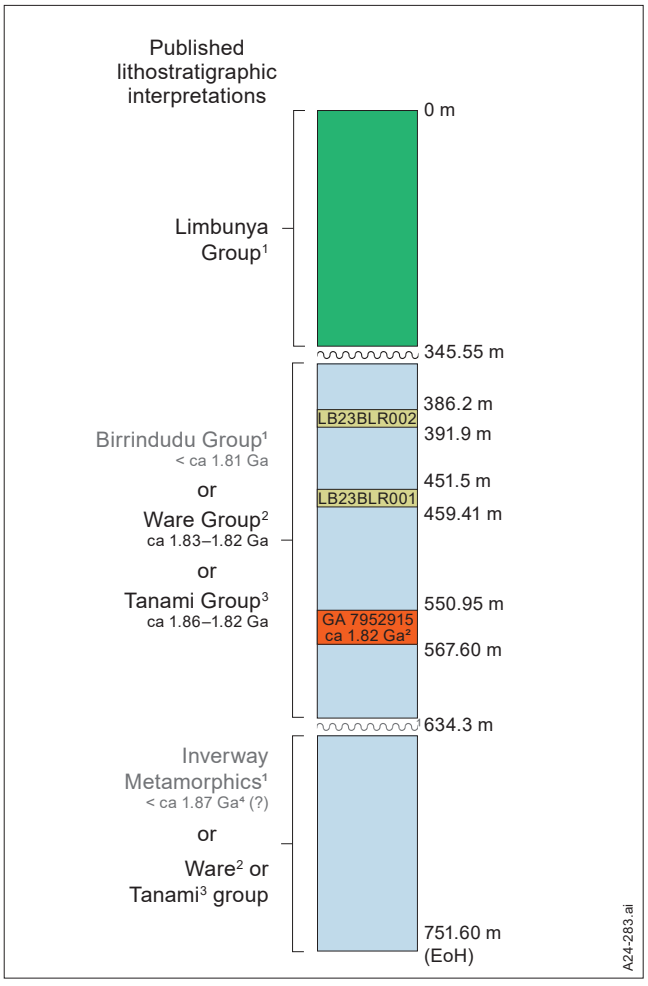

Figure 4. Simplified geological log of drillhole LBD2 after Kositcin and Carson (2024). The log depicts the high level stratigraphy interpreted by Muir (2011), the revised stratigraphy proposed by Kositcin and Carson (2024) and the location of the two samples discussed in this Record. Grey text represents interpretations that are now considered unlikely.
[1] preferred interpretation of Muir (2011)
[2] preferred interpretation of Kositcin and Carson (2024)
[3] alternate interpretation of Kositcin and Carson (2024)
[4] Kositcin and Carson (2017)

The interpretation of Inverway Metamorphics at the base of the hole was based on the presence of that unit ~19 km south-west of the drillhole location. Kositcin and Carson (2017) interpreted the Inverway Metamorphics to have a maximum depositional age of ca 1.87 Ga but also raised the possibility of the sample representing a correlative of the Tanami Group. But the sample location, photograph and description of the sample in Kositcin and Carson (2017) is also consistent with the sample instead belonging to the Stirling Sandstone of the Limbunya Group of the Birrindudu Basin.

The age of the Birrindudu Group is constrained to be younger than ca 1.77 Ga, based on the age of the underlying Pargee Sandstone (Cross and Crispe 2007), and older than ca 1.65 Ga, based on the age of the overlying Limbunya Group (Fanning 1991).

Maximum depositional ages in the Limbunya Group are in the range ca 1.83–1.64 Ga (Dunster and Ahmad 2013), and a tuff in the Fraynes Formation near the top of the Limbunya Group provides a constraint of ca 1.64 Ga on the depositional age for that formation (Munson *et al* 2019).

Subsequent studies have suggested alternative interpretations of the stratigraphy intersected in LBD2. Schmid and Baumgartner (2024) found that rocks below the Limbunya Group between ~350 m and ~500 m include hydrothermally altered and metamorphosed mafic volcaniclastic rocks, inconsistent with Birrindudu Group stratigraphy. Kositcin and Carson (2024) obtained a SHRIMP U–Pb zircon age of ca 1.82 Ga for a feldspar porphyry sill at 562.50–563.00 m depth, which is older than the age range of the Birrindudu Group and would require the units beneath the ~345.55 m unconformity to be older than ca 1.82 Ga.

Accordingly, the identity and age of the units below the unconformity at the base of the Limbunya Group in LBD2 remain poorly constrained. Kositcin and Carson (2024) present multiple hypotheses for an alternative stratigraphic interpretation, with a preferred model that assigns all the rocks below a depth of 345.55 m to the Ware Group of the Tanami Region. Other hypotheses include correlation with the Tanami Group of the Tanami Region, or with units of the Pine Creek Orogen. The identity of the rocks interpreted by Muir (2011) as Inverway Metamorphics remains untested.

In this study, two samples were taken from drillhole LBD2 in the Birrindudu Basin to provide additional constraints: sample LB23BLR001 in the interval 451.5–459.41 m, and sample LB23BLR002 in the interval 386.2–391.9 m. These intervals were logged by Muir (2011) as metashale with quartz, cordierite, biotite, andalusite, chlorite, pyrite, graphite and chalcopyrite; they are in the interval interpreted by Schmid and Baumgartner (2024) as mafic volcaniclastic rocks.

LB23BLR001

Sample information

Sample ID: LB23BLR001
Collector: Barry Reno
1:250 000 mapsheet: LIMBUNYA
1:100 000 mapsheet: Gregorys Depot
Province/Region: unassigned
Longitude (GDA94): 130.128319
Latitude (GDA94): -17.46228
Drill hole: LBD2
Depth from (m): 451.5
Depth to (m): 459.41
Formal name: unassigned
Lithology: meta-mudstone

Interpreted age summary

Fabric development: at or after ca 1.86–1.70 Ga
Thermal overprint: ca 1.62 Ga
Thermal, hydrothermal, or alteration: 234 ± 34 Ma

Sample context

Sample LB23BLR001 is a mudstone that records an amphibolite facies metamorphic overprint (see Ashley *et al* 2025 for a detailed petrographic description). The interval is compositionally layered (**Figure 5**) with layers defined by variable amounts of graphite (**Figure 6**). A thin section from 459.0 m within the sampled interval reveals an early metamorphic assemblage, comprising cordierite–muscovite–quartz–graphite±rutile, that forms a weak grain shape fabric defined by graphite and cordierite oriented co-planar to compositional layering. Andalusite (**Figure 6**) and rutile (**Figure 7a,b**) form randomly-oriented elongate porphyroblasts that overprint both the grain shape fabric defined by the early metamorphic assemblage and the compositional layering; the size and number of porphyroblasts relates to local composition within the interval, with andalusite laths up to 5–8 mm in length, and rutile up to 300 µm in length. Andalusite porphyroblasts have an inclusion assemblage of graphite and rutile (**Figure 7c**). Andalusite and cordierite are both retrogressed and generally occur as pseudomorphs of sericite ± clay replacing andalusite or cordierite. Minor sub-mm wide quartz veins (**Figure 5**) and faults (**Figures 5, 6**) are discordant from the compositional layering, the fabric, and the andalusite porphyroblasts. Rutile is estimated to be approximately 1% by volume of the rock. Rutile separated from the entire interval includes both laths and irregular shaped or ovoid shaped grains up to 1 mm in diameter.

Analytical results

A total of 100 analyses were carried out on rutile separated from sample LB23BLR001. The isotope data are presented in **Appendix 1** and **Figures 8**–**11**. A plot of Sn and Nb for all analyses (**Figure 8a**) reveals two discrete rutile populations: Population 1 that forms a cluster of 47 analyses with Nb of 750–1500 ppm; and Population 2 that forms a cluster of 40 analyses with Nb < 350 ppm and Sn < 23 ppm. Likewise, a

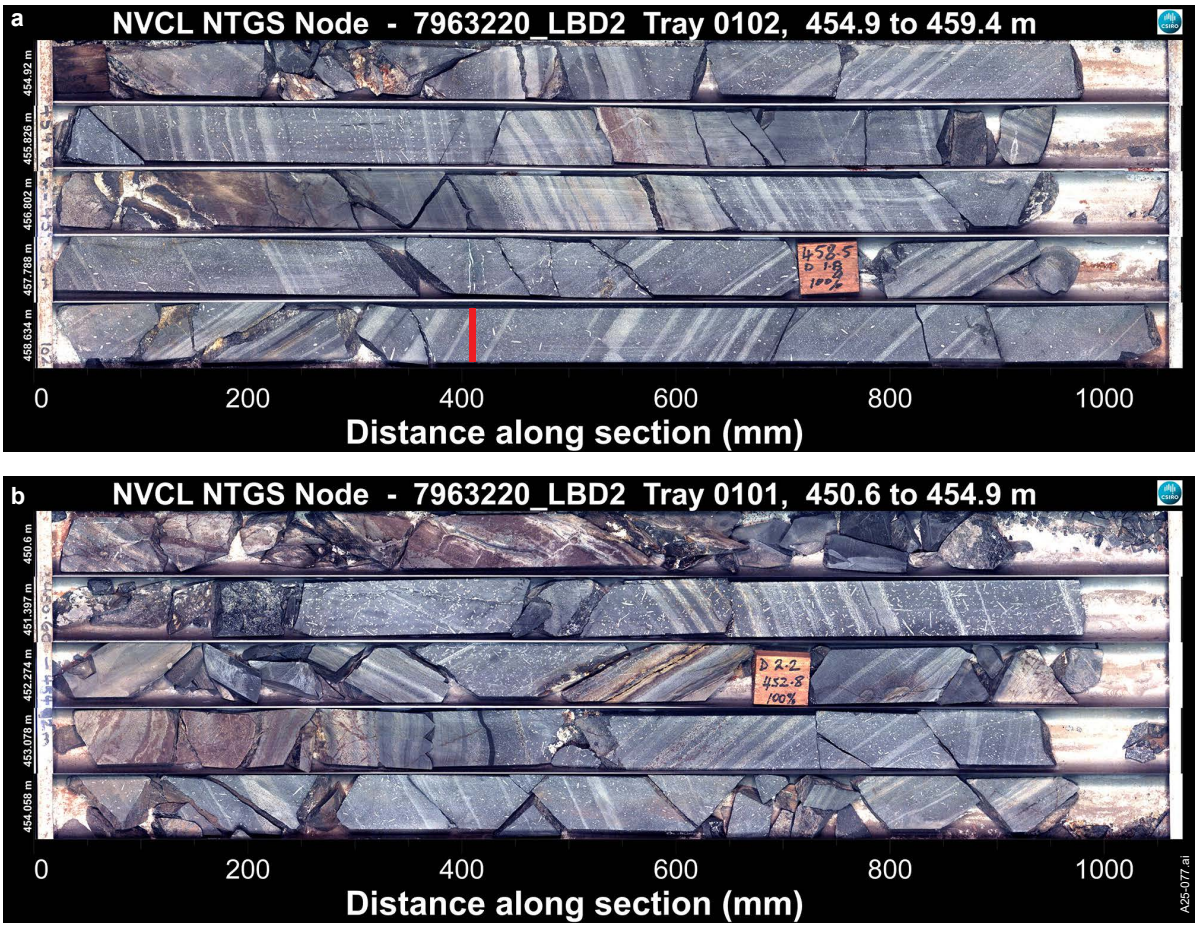

Figure 5. Selected HyLogger core imagery of drillhole LBD2, showing sampled interval (451.5–459.41 m).

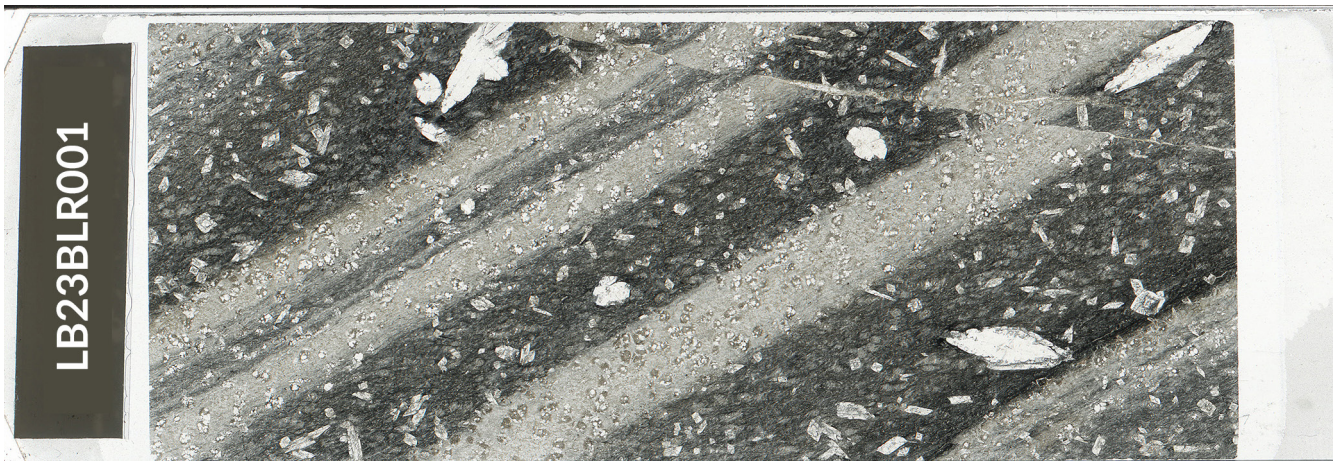

Figure 6. Thin section of sample LB23BLR001 from 459.0 m depth within the sampled interval of drillhole LBD2. The dark and light banding relates to the amount of graphite in the sample and the transparent lath or diamond shaped porphyroblasts are sericite±clay-after-andalusite.

plot of Zr and Nb for all analyses (**Figure 8b**) shows that Zr concentration varies between the populations: Population 1 having a narrow range of Zr, with 80% of Population 1 having Zr concentrations between 236–352 ppm; and Population 2 having a wider range of Zr concentration that spans 4 orders of magnitude in the range ~50–11 000 ppm. Thirteen analyses are outliers and not included in either population.

A concordia plot shows that the two chemical populations define two distinct common Pb age trends (**Figure 9**): Population 1 defines a trend with a lower intercept 1645 ± 47 Ma; and Population 2 defining a trend with a lower intercept at 243 ± 34 Ma. The two rutile populations have identical (or very similar) common Pb sources, with $(^{207}Pb/^{206}Pb)_c$ of 0.763 ± 0.007 for Population 1 and 0.755 ± 0.008 for Population 2 (**Figure 9**). A kernel density estimate (KDE) using concordia calculated for each analysis by projecting an isochron from the common Pb composition through each individual analysis to the concordia line is shown in **Figure 10**. The KDE reveals that Population 1 is not normally distributed, and instead has a clear peak and an older tail; this indicates that the isochron fit through this population is a maximum estimate for the peak, and that the main age component in Population 1 is younger than the isochron lower intercept age of ca 1.65 Ga (**Figure 10**). The discrete mixture modelling algorithm of Galbraith and Laslett (1993), using the Bayes Information Criteria to choose the number of peaks (Vermeesch 2018), gives modelled age components of 1863 ± 6 Ma (13%), 1792 ± 1 Ma (12%), 1697 ± 1 Ma (28%), 1617 ± 3 Ma (34%), and 1504 ± 2 Ma (12%) (**Figure 11**).

Interpretation

There are multiple populations of rutile in sample LB23BLR001 that are clearly defined by a combination of petrographic setting, trace element chemistry, and age.

On a Tera-Wasserburg concordia diagram the two chemical populations correspond to two distinct common lead trends that both originate from the same initial common Pb composition: Population 1 with a lower intercept of ca 1643 Ma and Population 2 with a lower intercept of ca 243 Ma (**Figure 9**).

A KDE of projected concordia ages reveals that Population 1 is not normally distributed, and instead has a strong peak and an older tail. This indicates that the lower intercept age is a maximum estimate for the main peak, and that the main peak is younger than ca 1.65 Ga. The ca 1.62 Ga age component from mixture modelling best estimates the peak and is interpreted to represent the main age component in Population 1. The uncertainty of ± 3 Ma on that age component represents the uncertainty on the peak deconvolution and does not fully estimate geological or analytical uncertainty; the true uncertainty is higher than this but is not estimated here.

Population 2 forms a single age peak with the lower intercept age of 234 ± 34 Ma interpreted to best estimate the age for this population.

Petrography shows that rutile occurs in two main settings: an older setting where rutile occurs as inclusions in porphyroblasts or is aligned in the fabric, and a younger population where rutile is randomly oriented and overprints the fabric. As age data presented here was collected from mineral separates and not *in situ*, it is not possible to directly link the two petrographic populations to ages.

Nonetheless, there are several key interpretations that can be made confidently:

1. The older age populations associated with the older age tail on Population 1 (eg, the mixture model ages of ca 1.86 Ga, 1.79 Ga and 1.67 Ga) most likely pre-date, or represent the timing of fabric development in the rock. The specific ages may not have geological meaning but are instead consistent with rutile that spans these ages.
2. The main ca 1.62 Ga peak most likely represents a (hydro-)thermal overprint. This age likely post-dates the timing of fabric development because the overlying ca 1.64 Ga Limbuya Group rocks are undeformed.
3. The youngest age of ca 243 Ma post-dates fabric and andalusite development, and represents rutile associated with a (hydro-)thermal overprint. This overprint was not sufficient to reset the U–Pb system in rutile throughout the rock and could represent the timing of the minor discordant quartz veins and faults (**Figures 5, 6**) observed in the interval.

Future *in situ* analysis may further resolve the individual age components in the old tail and provide evidence to constrain the timing of deformation.

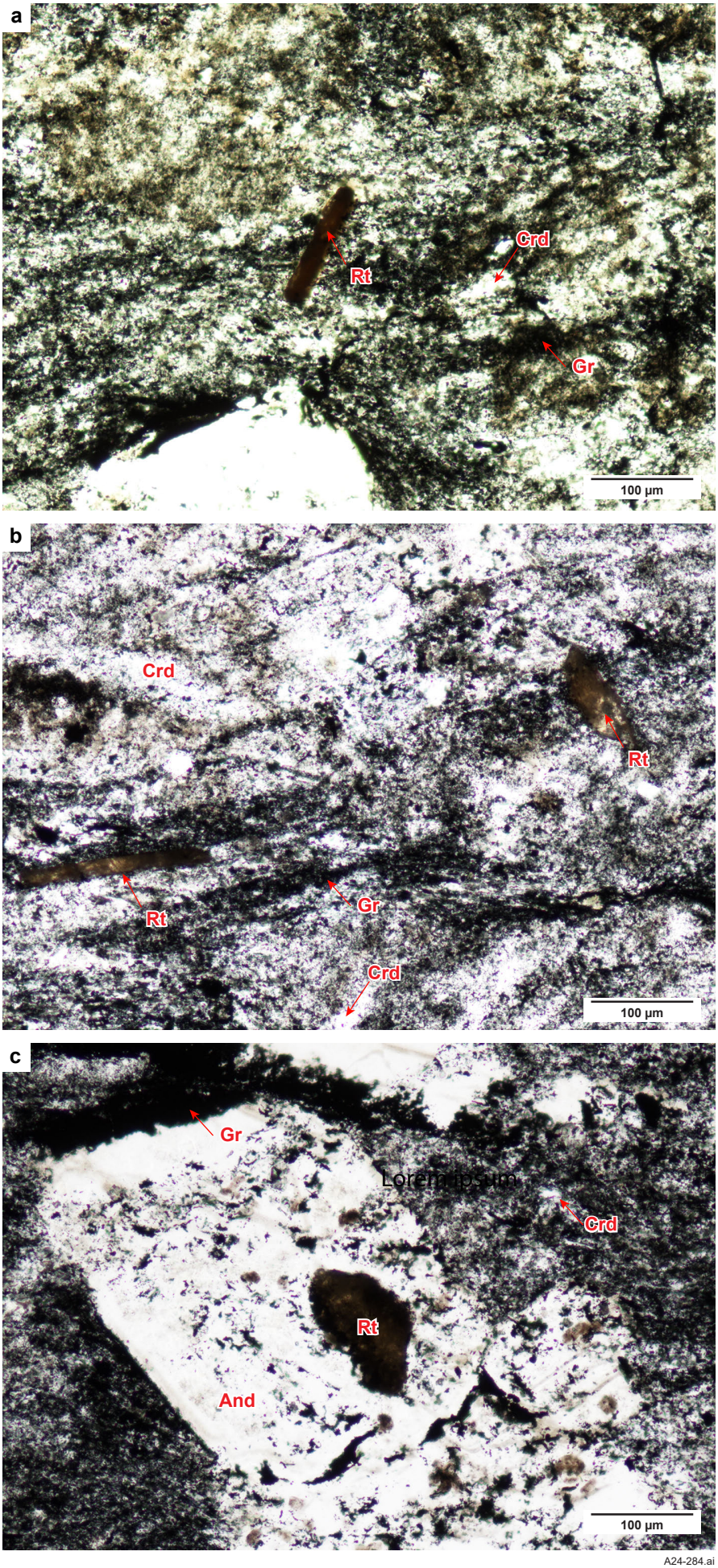

Figure 7. Plane-polarised photomicrographs of rutile in sample LB23BLR001. (**a**) and (**b**) show examples of randomly-oriented rutile that overprints the graphite fabric; (**c**) is an example of rutile inclusion in a sericite-after-andalusite porphyroblast.

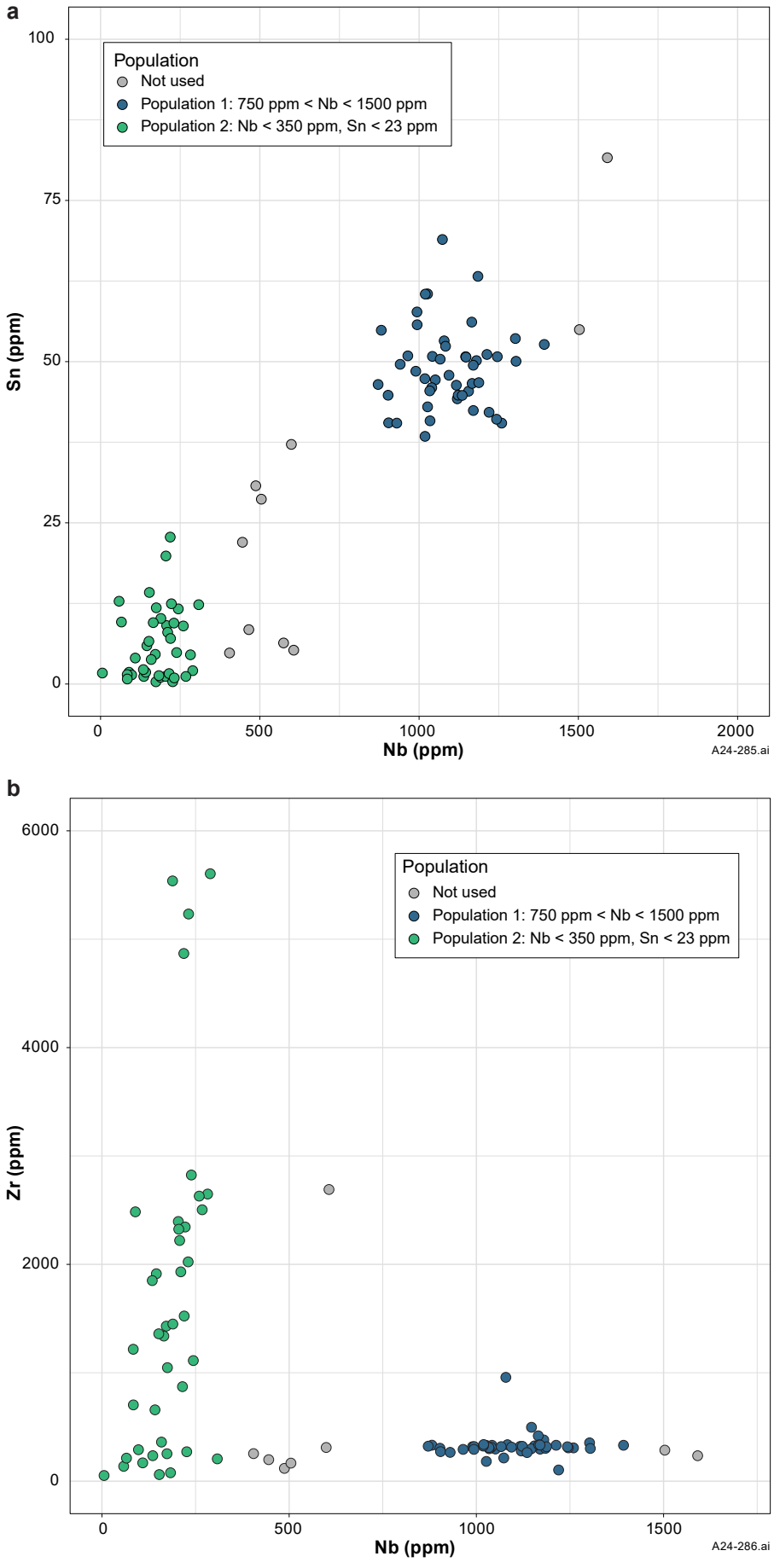

Figure 8. (**a**) Sn vs Nb and (**b**) Zr vs Nb chemistry for rutile in sample LB23BLR001. Points are coloured by the populations discussed in the text.

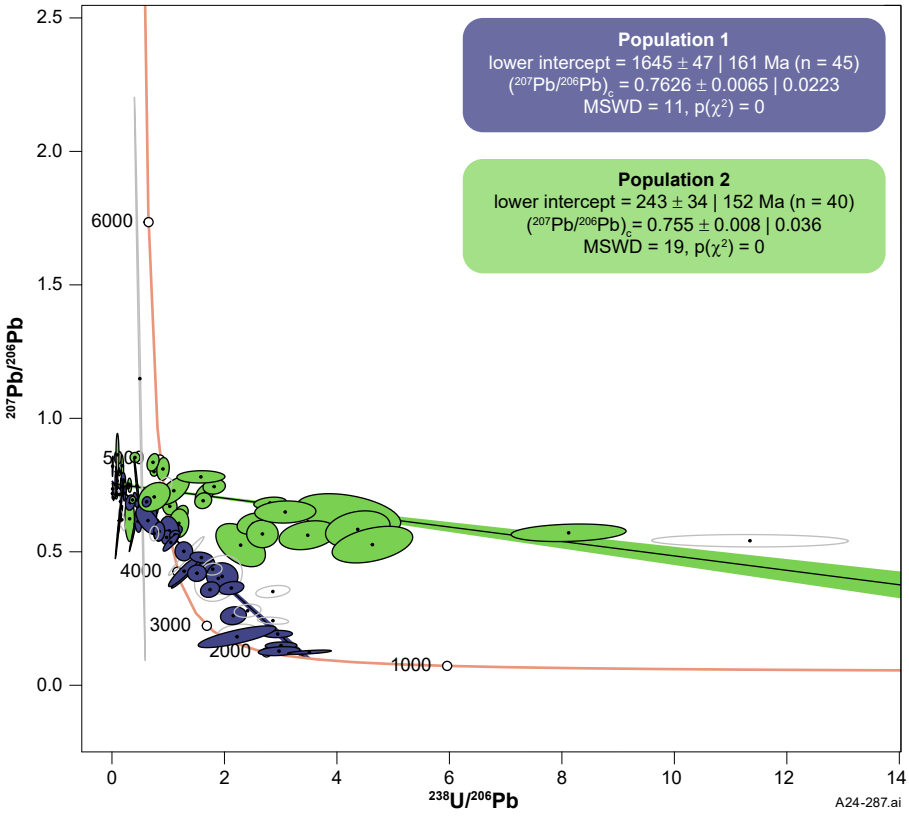

Figure 9. Tera-Wasserburg concordia diagram for rutile in sample LB23BLR001. Black dots show individual isotope analyses, and the ellipses show 2σ confidence intervals. Ellipses and discordia are coloured based on the populations discussed in the text, with blue ellipses representing the low-Nb-low-Sn population, and green ellipses representing the high-Nb-high-Sn population. Unfilled ellipses were excluded from age calculations. The black lines are discordia through the data calculated using the maximum likelihood algorithm of Ludwig (1998); the green and blue buffers show 95% confidence intervals on the regressions. The uncertainties on the lower intercept and common lead calculations are 2σ absolute uncertainties, and 2σ absolute uncertainties augmented by √mswd to account for any overdispersion.

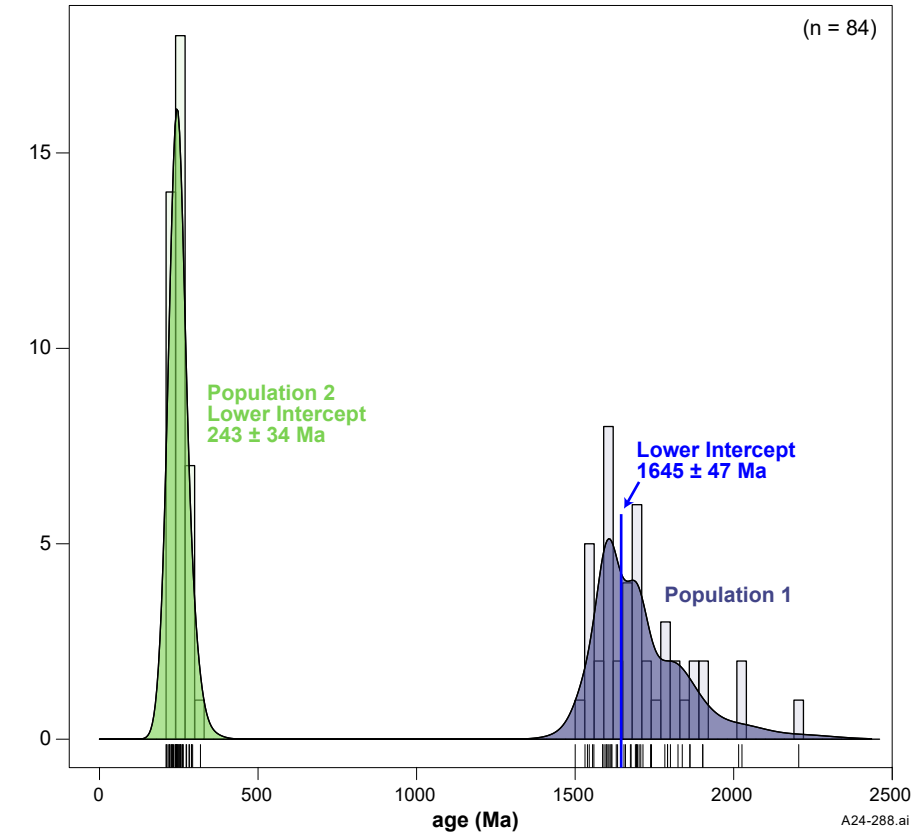

Figure 10. Kernel density estimate (curves) and histogram (bars) for concordia ages from sample LB23BLR001 calculated using the common.Pb = 2 method in IsoplotR; this method removes common Pb by projecting data along an inverse isochron from the calculated common Pb composition for each analysis point.

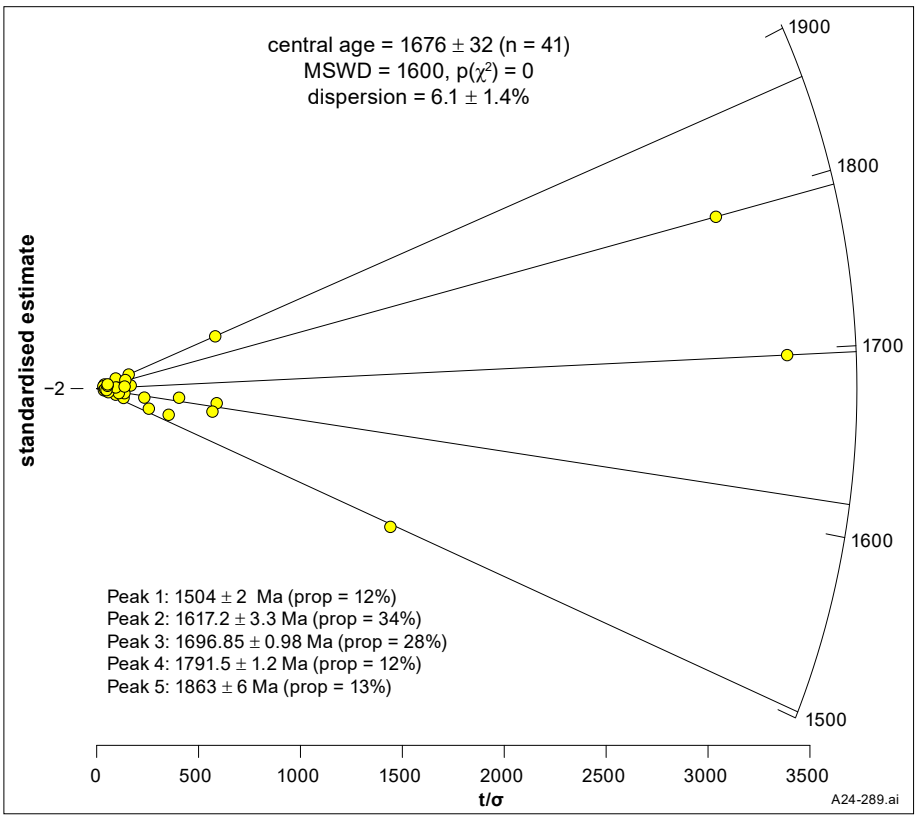

Figure 11. Radial plot and discrete mixture modelling results for Population 1 of the rutile data from sample LB23BLR001.

LB23BLR002

Sample information
Sample ID: LB23BLR002
Collector: Barry Reno
1:250 000 mapsheet: LIMBUNYA
1:100 000 mapsheet: Gregorys Depot
Province/Region: unassigned
Longitude (GDA94): 130.128319
Latitude (GDA94): -17.46228
Drill hole: LBD2
Depth from (m): 386.2
Depth to (m): 391.9
Formal name: unassigned
Lithology: metatuff or metamudstone

Interpreted age summary
Volcanism or maximum deposition, or recrystallisation: ca 2.06 Ga
Metamorphism: ca 1.72 Ga

Sample context

Sample LB23BLR002 was taken from an interval of fine-grained, cream-colored meta-sedimentary rock in drillhole LBD2 (**Figure 12**). The interval has mm- to cm-scale bedding defined by Fe-staining within the rock, probably due to variable hematite composition or sulphide veins. Joints and cracks within the interval are Fe-altered. A thin section from a depth of 391.0 m (within the sampled interval) is sericite-rich with subordinate intergrown quartz-hematite, minor chlorite, and trace carbonate minerals (**Figure 13**). The interval has a low-grade metamorphic overprint that led to pervasive fine-grained recrystallisation of all phases obscuring primary sedimentary microstructures. Based on sample mineralogy, Ashley *et al* (2025) speculate that the interval is either an altered fine-grained tuff or has an Fe-rich mudstone protolith. Although neither rutile or zircon were observed in thin section below a depth of 391 m, the mineral separate from the whole interval yielded abundant rutile up to 120 µm in diameter; individual rutile grains had both equant ovoil or sub-round, and elongate lath-like grain shapes. Forty-seven zircon grains large enough for analysis were found, with the largest grains 50–100 µm in diameter. Individual zircon grains include a range of grain morphologies including euhedral laths, ovoid shaped grains and irregularly shaped grains. CL imagery reveals a range of internal zonation patterns, including concentric, patchwork and irregular, and some grains have distinct cores and rims.

Analytical results – rutile

A total of 208 analyses were carried out on rutile from sample LB23BLR002. The isotope data are presented in **Appendix 1** and **Figures 14**–**17**. A plot of Sn and Nb, shaded using the zirconium concentration for all rutile analyses (**Figure 14**), shows that most analyses form a tight cluster with Nb concentrations in the range 400–750 ppm and Sn <5 ppm. However, there is also a spread of data to higher Sn or higher Nb contents and trace element chemistry does not reveal any clear populations.

A concordia plot reveals that the rutile data form a clear but broad common Pb age trend (**Figure 15**). An isochron fit through the data has a lower intercept at 2094 ± 26 Ma, and a common lead composition of $(^{207}Pb/^{206}Pb)_c$ of 0.940 ± 0.004. A kernel density estimate (KDE) using concordia dates calculated for each analysis, done by projecting an isochron from the common Pb composition through each individual analysis to the concordia line, is shown in **Figure 16**. The KDE reveals that the ages are not normally distributed, but instead have a major peak at around 2.0 Ga, a substantial older tail, and a discrete, subordinate, younger peak; this indicates that the isochron fit through this population is most likely a maximum estimate for the peak, and that the main age in this population is younger than the isochron lower intercept age of ca 2.09 Ga. The discrete mixture modelling algorithm of Galbraith and Laslett (1993), using the Bayes Information Criteria to choose the number of peaks (Vermeesch 2018), gives modelled age components of 3022 ± 51 Ma (3%), 2645 ± 10 Ma (20%), 2205 ± 5 Ma (30%), 2057 ± 3 Ma (38%), and 1717 ± 29 Ma (9%) (**Figure 17**).

Analytical results – zircon

A total of 46 analyses were carried out on zircons separated from sample LB23BLR002. The isotope data are presented in **Appendix 1** and **Figure 18**. All but one grain analysed appear to be metamict – with increased concentrations of Fe, La, Ti, and P – and experienced Pb loss and/or addition of common Pb. A concordia plot (**Figure 18**) does not

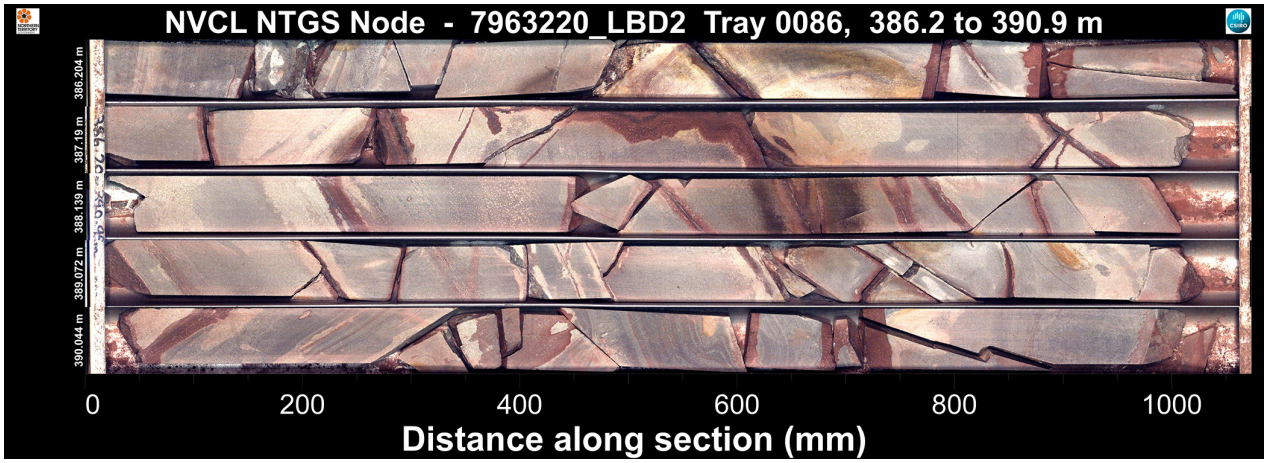

Figure 12. Selected HyLogger core imagery of drillhole LBD2 showing sampled interval (386.2–391.9 m).

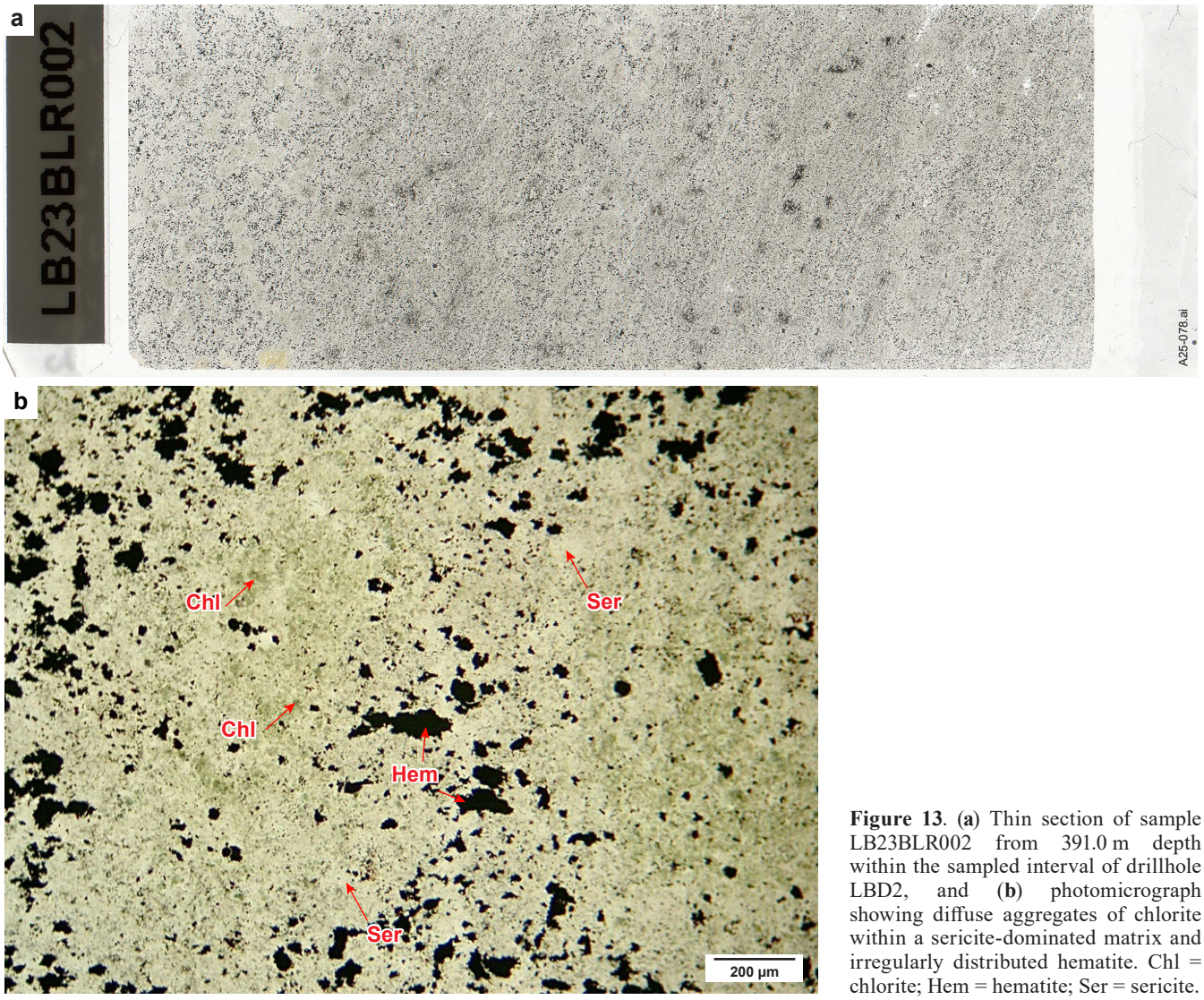

Figure 13. (**a**) Thin section of sample LB23BLR002 from 391.0 m depth within the sampled interval of drillhole LBD2, and (**b**) photomicrograph showing diffuse aggregates of chlorite within a sericite-dominated matrix and irregularly distributed hematite. Chl = chlorite; Hem = hematite; Ser = sericite.

reveal a clear trend. A single concordant analysis for a non-metamict grain has a $^{207}Pb/^{206}Pb$ date of 1919 ± 10 Ma.

Interpretation

Based on rutile chemistry, there is no clear way to identify distinct populations in the data. Moreover, there was no rutile found in the thin section for sample LB23BLR002. As such, there are no petrographic or microstructural constraints on rutile petrogenesis. A KDE plot of projected concordia shows that the data are not normally distributed, with a main age peak at around 2 Ga, an older tail, and a discrete younger population around 1.7 Ga. Accordingly, the lower intercept age ca 2.09 Ga is not geologically meaningful because it is an average of all populations. Instead, the ca 2.06 Ga age component from mixture modelling best estimates the peak and is interpreted to represent the main age component. The uncertainty of ± 3 Ma on that age component represents the uncertainty on the peak deconvolution and does not fully estimate geological or analytical uncertainty; the true uncertainty is higher than this but is not estimated here.

The sampled interval was interpreted by Schmid and Baumgartner (2024) to have a metamorphosed or hydrothermally altered volcaniclastic protolith, consistent with the petrographic observation of a pervasively recrystallised volcaniclastic rock or Fe-rich mudstone by Ashley *et al* (2025). The old tail in the rutile KDE is consistent with the sample having an inherited component.

If the interpretation that the rock has a volcaniclastic protolith is correct, then it is likely that rutile would preserve chronologic evidence for both: (1) volcanism (and so by proxy deposition); and (2) the pervasive recrystallisation experienced by the sample. The two most probable ways to interpret the ages given these observations are:

1. The main peak at ca 2.06 Ga could record the timing of rutile crystallisation during volcanism, in which case the pervasive recrystallisation occurred at ca 1.72 Ga.
2. The pervasive recrystallisation could have had a significant effect on rutile in the sample. If so, the main peak at ca 2.06 Ga could record the timing of pervasive recrystallisation. In this case, the timing of volcanism and deposition would be older than ca 2.06 Ga, and the younger ca 1.72 Ga peak would relate to a younger overprint, similar to that experienced by sample LB23BLR001.

If the hypothesis that the interval is volcaniclastic is incorrect, the deposition ages would instead be interpreted as a maximum deposition ages.

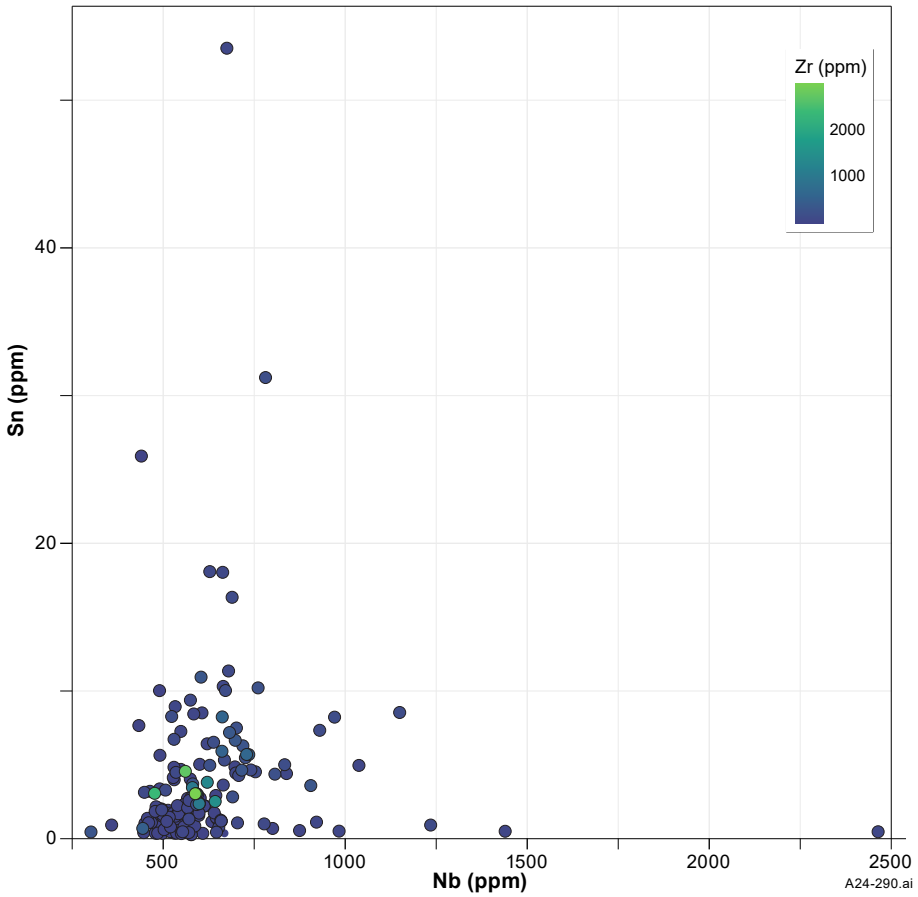

Figure 14. Sn vs Nb chemistry, coloured by zirconium concentration for rutile in sample LB23BLR002.

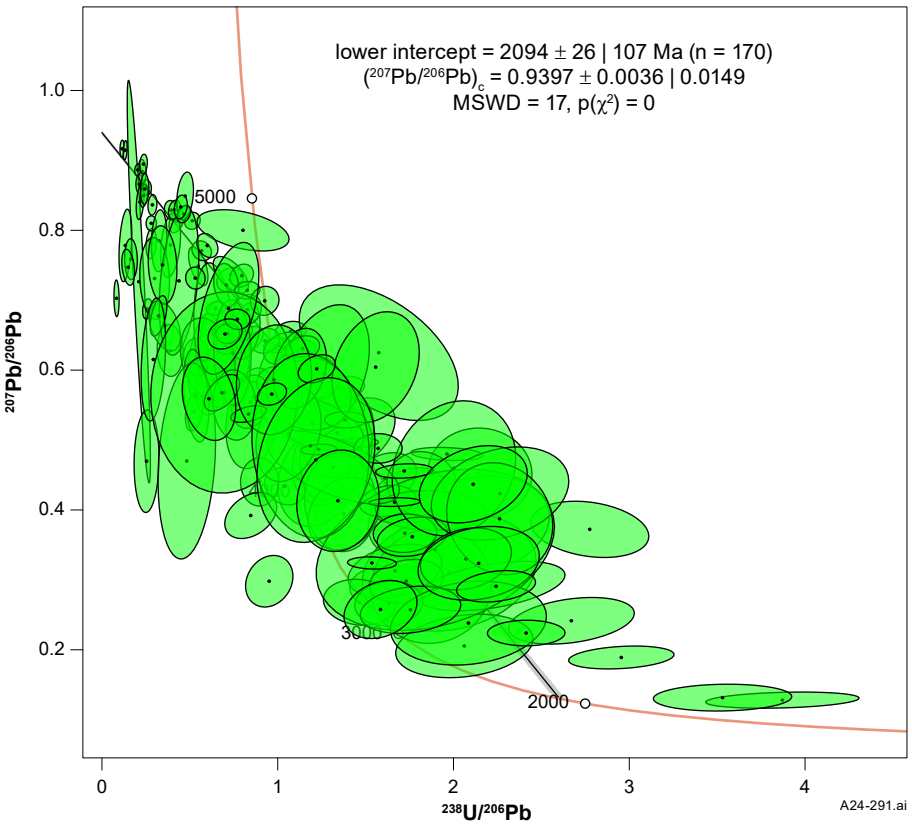

Figure 15. Tera-Wasserburg concordia diagram for rutile in sample LB23BLR002. Black dots show individual isotope analyses, and the ellipses show 2σ confidence intervals. The black line is a discordia through the data calculated using the maximum likelihood algorithm of Ludwig (1998), and the grey buffer shows a 95% confidence interval on the regression. The uncertainties on the lower intercept and common lead calculations are 2σ absolute uncertainties, and 2σ absolute uncertainties augmented by √mswd to account for any overdispersion.

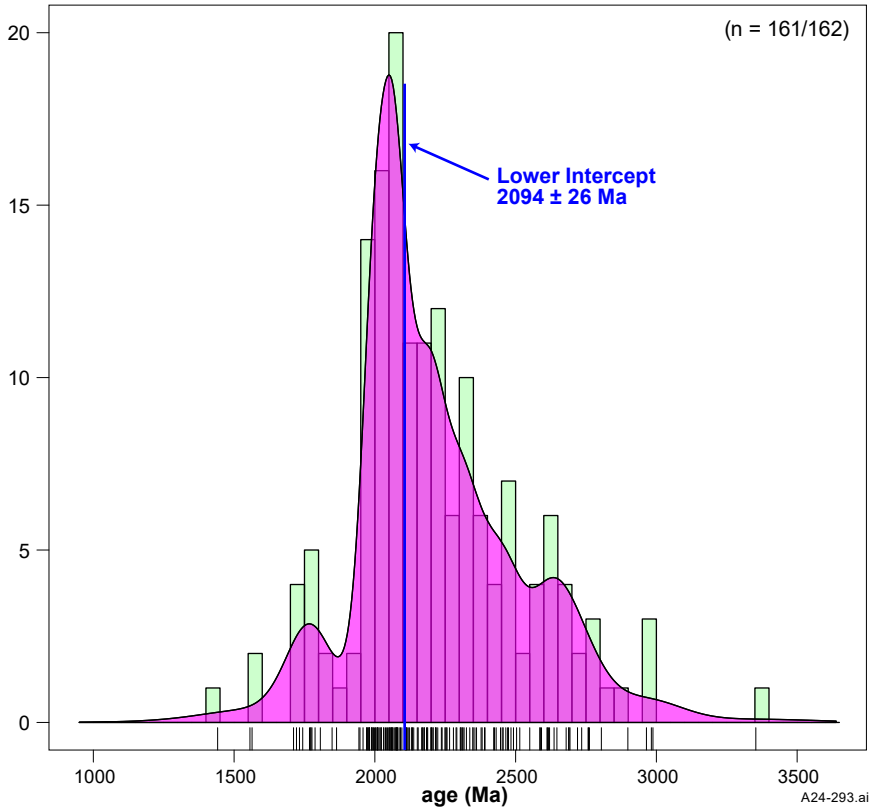

Figure 16. Kernel density estimate (curve) and histogram (bars) for concordia ages from sample LB23BLR002 calculated using the common.Pb = 2 method in IsoplotR; this method removes common Pb by projecting the data along an inverse isochron from the calculated common Pb composition for each analysis point.

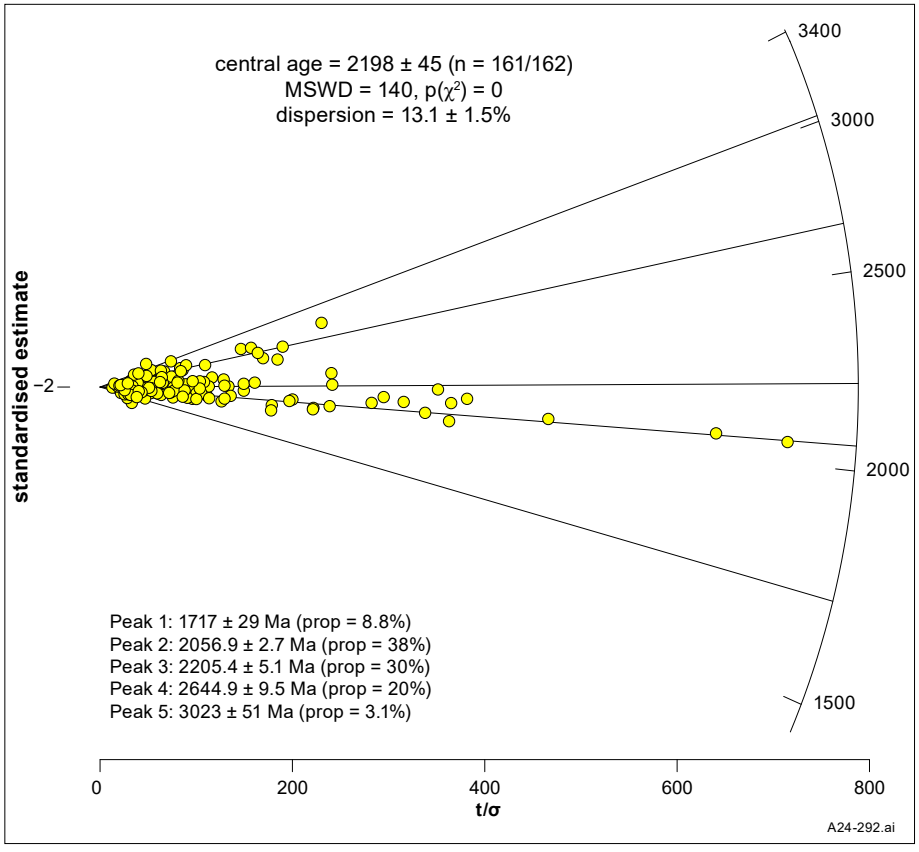

Figure 17. Radial plot and discrete mixture modelling results for rutile data from sample LB23BLR002.

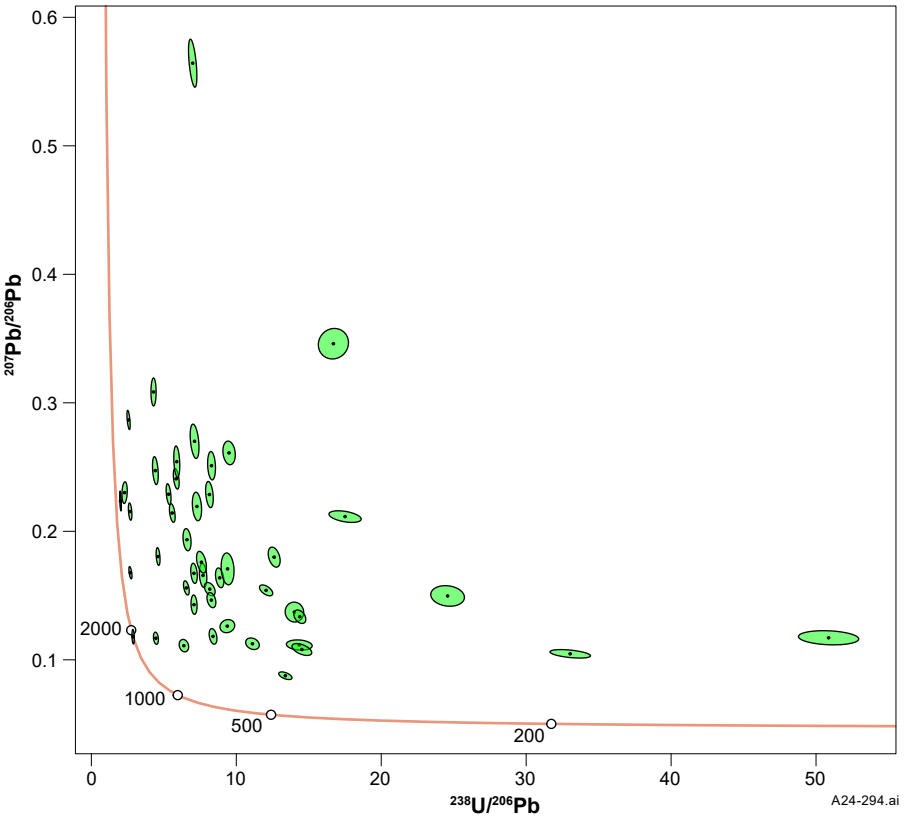

Figure 18. Tera-Wasserburg concordia diagram for zircon in sample LB23BLR002. Black dots show individual isotope analyses, the ellipses show 2σ confidence intervals.

Implications for LBD2

The rutile and zircon chronologic data presented here, together with that of Kositcin and Carson (2024), suggest that the basement to the Limbunya Group below 345.55 m in drillhole LBD2 is likely older than the Ware or Tanami groups (**Figures 19, 20**).

The rutile age of approximately 2.06 Ga comes from a pervasively recrystallised interval with a likely volcaniclastic protolith (Schmid and Baumgartner 2024, Ashley *et al* 2025). There are two probable interpretations for this age: (1) it may record the timing of volcanism and sample deposition; or (2) it may record pervasive metamorphism and recrystallisation. A deposition age of, or older than, ca 2.06 Ga suggests that the interval does not belong to any known lithostratigraphic unit within the Tanami Region (**Figure 20**). It may instead correlate with the Woodcutters Supergroup in the Pine Creek Orogen – which is suggested to be ca 2.02 Ga based on limited zircon data (**Figure 20**; Worden *et al* 2004, Worden *et al* 2008) – or it may represent an older stratigraphic unit. However, this correlation is tentative and further data are needed. This age also provides a minimum deposition age for the rocks deeper than ~391.9 m.

A third possible interpretation is that ca 2.06 Ga age represents a maximum deposition age for the sample; this is considered a less likely scenario given the volcaniclastic nature of the protolith and evidence for pervasive recrystallisation of the sample.

The ca 2.06 Ga rutile age from 391.9 m indicates that the basement of LBD2 below 634.4 m cannot be the same unit interpreted as Inverway Metamorphics by Kositcin and Carson (2017) and cannot be correlative of the ca 1.86–1.82 Ga (Ahmad *et al* 2013) Tanami Group (**Figure 20**). Further work is required to establish the units' age and identity.

Both samples experienced at least one metamorphic overprint. Sample LB23BLR001 preserves a grain shape foliation defined by graphite and cordierite, along with some rutile. It also shows a late thermal overprint defined by randomly-oriented andalusite and rutile that overprints the graphite-cordierite fabric. The older tail between around 1.8 and 1.7 Ga may record fabric development in sample LB23BLR001. The youngest peak of approximately 1.72 Ga in LB23BLR002 would relate to recrystallisation of that sample if the deposition age is ca 2.06 Ga, or otherwise to a later thermal or deformation event. This age range

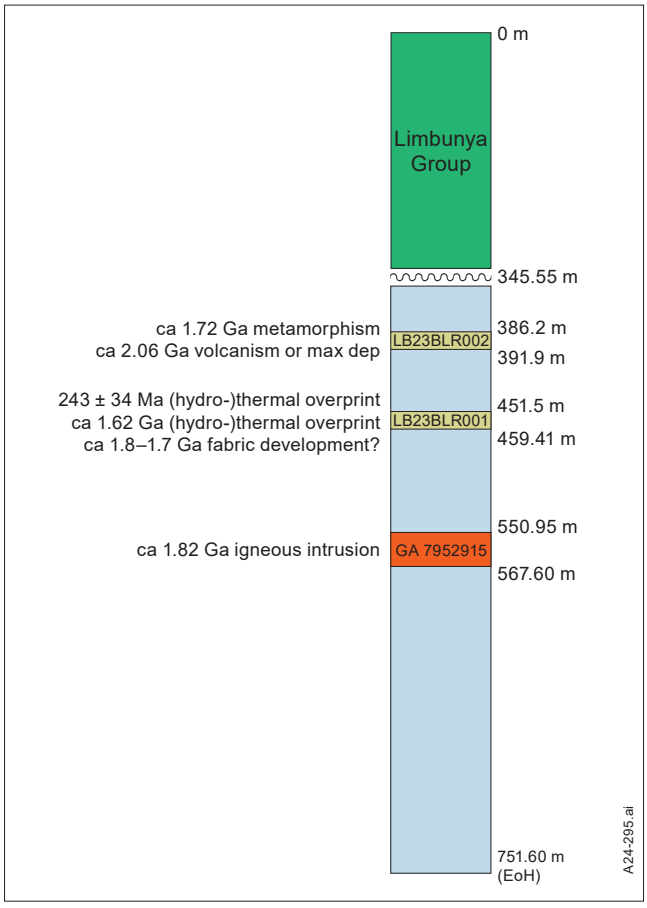

Figure 19. Simplified geological log of drillhole LBD2 after **Figure 2**, summarising the available chronologic data. Previously published interpretations now considered unlikely are not shown. A volcanic age of ca 2.06 Ga for sample LB23BLR002 would require the interval beneath the Limbunya Group to be older than either the Ware or Tanami groups of the Tanami Region. Regionally, it might be coeval with the Woodcutters Supergroup. Further work is required to confidently assign an age and lithostratigraphic interpretation to this interval.

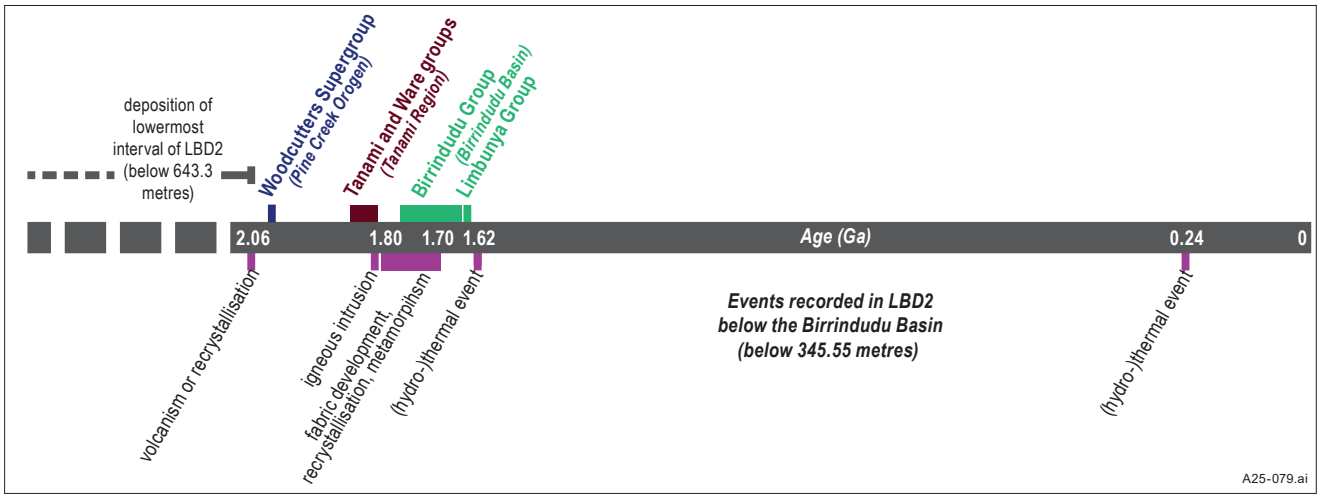

Figure 20. Timeline of events experienced by rocks below the unconformity with the overlying Birrindudu Basin (at 345.55 m) in drillhole LBD2. The events shown in italic black text at the bottom of the timeline are based on data from this Record except for the ca 1.82 Ga igneous intrusion age of Kositcin and Carson (2024). The timing of deposition of regional stratigraphic units is indicated by bold colour text above the timeline.

indicates that this terrane was affected by tectonic events that occurred regionally throughout the North Australian Craton at this time (eg Ahmad and Scrimgeour 2013).

The youngest Proterozoic age of ca 1.62 Ga in sample LB23BLR001 likely post-dates deformation, as the overlying undeformed Limbunya Group is known to have been deposited by ca 1.64 Ga (**Figure 20**). This suggests a thermal or hydrothermal overprint at around 1.62 Ga that may record the timing of andalusite porphyroblast development potentially related to subsidence associated with development of the overlying Birrindudu Basin. Further *in situ* geochronology is required to confirm this.

The youngest age of 234 ± 34 Ma indicates a thermal or hydrothermal event affected the sample during the Permian–Triassic. As this age is rare in this part of Australia the regional significance of this overprint is not yet clear. However, apatite fission track ages from the Pine Creek Orogen and the Arnhem Province show a strong age component of ca 400–200 Ma, which Nixon *et al* (2020) proposed to be related to mantle-induced subsidence and the onset of sedimentation on the Money Shoal Basin, as well as regional uplift as a far-field effect of orogenesis in the Tasmanides. Rocks of drillhole LBD2 are likely to have been affected by the same processes.

ACKNOWLEDGEMENTS

We thank Pablo Farias for his review of this record. We thank Susanne Schmid (CSIRO), Rafael Baumgartner (CSIRO), and Jade Anderson (Geoscience Australia) for helpful discussions. We thank Tom Medley (formerly of NTGS), Brad Newman (formerly of NTGS), and Darryl Stacey for their assistance at the Darwin Core Facility.

We acknowledge and pay our respects to the Aboriginal Traditional Owners responsible for the areas of study.

REFERENCES

Ahmad M and Scrimgeour IR, 2013. Chapter 2 - Geological framework: in Ahmad M and Munson TJ (compilers). *'Geology and mineral resources of the Northern Territory'. Northern Territory Geological Survey, Special Publication* 5.

Ashley PM, Reno BL and Farias PG, 2025. Petrographic characterisation of samples from the Pine Creek Orogen and drillhole LBD2, Northern Territory. *Northern Territory Geological Survey, Record* 2025-001.

Baker J, Peate D, Waight T and Meyzen C, 2004. Pb isotopic analysis of standards and samples using a ^{207}Pb–^{204}Pb double spike and thallium to correct for mass bias with a double-focusing MC-ICP-MS. *Chemical Geology* 211, 275–303. doi:10.1016/j.chemgeo.2004.06.030

Baldwin JA and Brown M, 2008. Age and duration of ultrahigh-temperature metamorphism in the Anápolis–Itauçu Complex, Southern Brasília Belt, central Brazil – constraints from U–Pb geochronology, mineral rare earth element chemistry and trace-element thermometry. *Journal of Metamorphic Geology* 26, 213–233. doi:10.1111/j.1525-1314.2007.00759.x

Black LP, Kamo SL, Allen CM, Davis DW, Aleinikoff JN, Valley JW, Mundil R, Campbell IH, Korsch RJ, Williams IS and Foudoulis C, 2004. Improved $^{206}Pb/^{238}U$ microprobe geochronology by the monitoring of a trace-element-related matrix effect; SHRIMP, ID–TIMS, ELA–ICP–MS and oxygen isotope documentation for a series of zircon standards. *Chemical Geology* 205, 115–140. doi:10.1016/j.chemgeo.2004.01.003

Chew DM, Petrus JA and Kamber BS, 2014. U–Pb LA–ICPMS dating using accessory mineral standards with variable common Pb. *Chemical Geology* 363, 185–199. doi:10.1016/j.chemgeo.2013.11.006

Cross AJ and Crispe AJ, 2007. SHRIMP U–Pb analyses of detrital zircon: a window to understanding the Paleoproterozoic development of the Tanami Region, northern Australia. *Mineralium Deposita* 42, 27–50. doi:10.1007/s00126-006-0102-6

Dunster JN and Ahmad M, 2013. Chapter 17 - Birrindudu Basin: in Ahmad M and Munson TJ (editors). *'Geology and mineral resources of the Northern Territory'. Northern Territory Geological Survey, Special Publication* 5.

Fanning CM, 1991. *Ion microprobe U-Pb zircon dating of a tuffaceous horizon within the Kunja Siltstone, Victoria River Basin, Northern Territory. Report for Pacific Oil and Gas Pty Ltd.* Australian National University, Research School of Earth Sciences.

Galbraith RF and Laslett GM, 1993. Statistical models for mixed fission track ages. *Nuclear Tracks and Radiation Measurements* 21, 459–470. doi:10.1016/1359-0189(93)90185-c

Garnier S, Ross N, Rudis B, Filipovic-Pierucci A, Galili T, timelyportfolio, O'Callaghan A, Greenwell B, Sievert C, Harris DJ, Sciaini M and Chen JJ, 2024. *{viridis(Lite)} - Colorblind-friendly color maps for R*. doi:10.5281/zenodo.4679423

Horstwood MSA, Košler J, Gehrels G, Jackson SE, McLean NM, Paton C, Pearson NJ, Sircombe K, Sylvester P, Vermeesch P, Bowring JF, Condon DJ and Schoene B, 2016. Community-Derived Standards for LA-ICP-MS U-(Th-)Pb Geochronology – Uncertainty propagation, age interpretation and data reporting. *Geostandards and Geoanalytical Research* 40, 311–332. doi:10.1111/j.1751-908X.2016.00379.x

Jenkins K, Goemann K, Belousov I, Morissette M and Danyushevsky L, 2023. Investigation of the ablation behaviour of andradite-grossular garnets and rutile with implications for U–Pb geochronology. *Geostandards and Geoanalytical Research* 47, 267–295. doi:10.1111/ggr.12478

Jochum KP, Wilson SA, Abouchami W, Amini M, Chmeleff J, Eisenhauer A, Hegner E, Iaccheri LM, Kieffer B, Krause J, McDonough WF, Mertz-Kraus R, Raczek I, Rudnick RL, Scholz D, Steinhoefel G, Stoll B, Stracke A, Tonarini S, Weis D, Weis U and Woodhead JD, 2011. GSD-1G and MPI-DING Reference glasses for *in situ* and bulk isotopic determination. *Geostandards and Geoanalytical Research* 35, 193–226. doi:10.1111/j.1751-908X.2010.00114.x

Kositcin N and Carson C, 2024. Exploring for the Future – SHRIMP U–Pb geochronology of drillhole LBD2, Limbunya region, Northern Territory. *Geoscience Australia, Record* 2024/20. doi:10.26186/149474

Kositcin N and Carson CJ, 2017. New SHRIMP U-Pb zircon ages from the Birrindudu and Victoria Basins, Northern Territory. *Geoscience Australia, Record* 2017/16. doi:10.11636/Record.2017.016

Ludwig KR, 1998. On the treatment of concordant uranium-lead ages. *Geochimica et Cosmochimica Acta* 62, 665–676. doi:10.1016/s0016-7037(98)00059-3

Luvizotto GL, Zack T, Meyer HP, Ludwig T, Triebold S, Kronz A, Münker C, Stockli DF, Prowatke S, Klemme S, Jacob DE and von Eynatten H, 2009. Rutile crystals as potential trace element and isotope mineral standards for microanalysis. *Chemical Geology* 261, 346–369. doi:10.1016/j.chemgeo.2008.04.012

Martin AJ, Gehrels GE and DeCelles PG, 2007. The tectonic significance of (U,Th)/Pb ages of monazite inclusions in garnet from the Himalaya of central Nepal. *Chemical Geology* 244, 1–24. doi:10.1016/j.chemgeo.2007.05.003

Muir M, 2011. Annual report EL25307 for year ending 28 December 2010. Proto Resources and Investments Ltd. *Northern Territory Geological Survey Open File Company Report* CR2010-1065.

Munson TJ, Denyszyn SW, Simmons JM and Kunzmann M, 2019. A 1642 Ma age for the Fraynes Formation, Birrindudu Basin, confirms correlation with the economically significant Barney Creek Formation, McArthur Basin, Northern Territory. *Australian Journal of Earth Sciences* 67, 321–330. doi:10.1080/08120099.2020.1669708

Nixon AL, Glorie S, Collins AS, Whelan JA, Reno BL, Danišík M, Wade BP and Fraser G, 2020. Footprints of the Alice Springs Orogeny preserved in far northern Australia: an application of multi-kinetic thermochronology in the Pine Creek Orogen and Arnhem Province. *Journal of the Geological Society* 178. doi:10.1144/jgs2020-173

Norris A and Danyushevsky L, 2018. Towards estimating the complete uncertainty budget of quantified results measured by LA-ICP-MS. *Goldschmidt Abstracts* 2018 1894.

Northern Territory Geological Survey, 2023. Compilation of 1:250 000 geology map series GIS. *Northern Territory Geological Survey, Digital Information Package* DIP 041.

Posit Team, 2024. *RStudio: Integrated development environment for R*. Boston, MA, Posit Software, PBC. http://www.posit.co/

R Core Team, 2024. *R: A language and environment for statistical computing*. Vienna, Austria, R Foundation for Statistical Computing. https://www.R-project.org/.

Reno BL, Piccoli PM, Brown M and Trouw RAJ, 2012. In situ monazite (U-Th)-Pb ages from the Southern Brasília Belt, Brazil: constraints on the high-temperature retrograde evolution of HP granulites. *Journal of Metamorphic Geology* 30, 81–112. doi:10.1111/j.1525-1314.2011.00957.x

Schmid S and Baumgartner R, 2024. First insights into the sediment-hosted copper mineral system of the Birrindudu Basin, NT – facies analysis and basement source rocks: in *'Annual Geoscience Exploration Seminar (AGES) Proceedings, Alice Springs, Northern Territory 16–17 April 2024'*. Northern Territory Geological Survey, Darwin, 68–72.

Schoene B, Condon DJ, Morgan L and McLean N, 2013. Precision and accuracy in geochronology. *Elements* 9, 19–24. doi:10.2113/gselements.9.1.19

Siivola J and Schmid R, 2007. List of mineral abbreviations. *IUGS Subcommission on the Systematics of Metamorphic Rocks*, 1–14.

Sláma J, Košler J, Condon DJ, Crowley JL, Gerdes A, Hanchar JM, Horstwood MSA, Morris GA, Nasdala L, Norberg N, Schaltegger U, Schoene B, Tubrett MN and Whitehouse MJ, 2008. Plešovice zircon – a new natural reference material for U–Pb and Hf isotopic microanalysis. *Chemical Geology* 249, 1–35. doi:10.1016/j.chemgeo.2007.11.005

Spencer CJ, Kirkland CL and Taylor RJM, 2016. Strategies towards statistically robust interpretations of *in situ* U–Pb zircon geochronology. *Geoscience Frontiers* 7, 581–589. doi:10.1016/j.gsf.2015.11.006

Thompson J, Meffre S, Maas R, Kamenetsky V, Kamenetsky M, Goemann K, Ehrig K and Danyushevsky L, 2016. Matrix effects in Pb/U measurements during LA-ICP-MS analysis of the mineral apatite. *Journal of Analytical Atomic Spectrometry* 31, 1206–1215. doi:10.1039/c6ja00048g

Thompson JM, Goemann K, Belousov I, Jenkins K, Kobussen A, Powell W and Danyushevsky L, 2021. Assessment of the mineral ilmenite for U–Pb dating by LA-ICP-MS. *Journal of Analytical Atomic Spectrometry* 36, 1244-1260. doi:10.1039/d1ja00069a

Vermeesch P, 2018. IsoplotR: A free and open toolbox for geochronology. *Geoscience Frontiers* 9, 1479–1493. doi:10.1016/j.gsf.2018.04.001

Vermeesch P, Resentini A and Garzanti E, 2016. An R package for statistical provenance analysis. *Sedimentary Geology* 336, 14–25. doi:10.1016/j.sedgeo.2016.01.009

Wickham H, 2016. *ggplot2: Elegant graphics for data analysis*. Springer-Verlag New York. https://ggplot2.tidyverse.org

Wickham H, François R, Henry L, Müller K and Vaughan D, 2023. *dplyr: A Grammar of data manipulation*. https://CRAN.R-project.org/package=dplyr

Wickham H, Vaughan D and Girlich M, 2024. *tidyr: Tidy messy data*. https://CRAN.R-project.org/package=tidyr

Wiedenbeck M, Allé P, Corfu F, Griffin WL, Meier M, Oberli F, Quadt AV, Roddick JC and Spiegel W, 1995. Three natural zircon standards for U-Th-Pb, Lu-Hf, trace element and REE analyses. *Geostandards and Geoanalytical Research* 19, 1–23. doi:10.1111/j.1751-908X.1995.tb00147.x

Worden KE, Carson CJ, Close DF, Donnellan NC and Scrimgeour IR, 2008. Summary of results. Joint NTGS–GA geochronology project: Tanami Region, Arunta Region, Pine Creek Orogen and Halls Creek Orogen correlatives, January 2005–March 2007. *Northern Territory Geological Survey, Record* 2008-003.

Worden KE, Claoué-Long JC, Scrimgeour IR and Lally JH, 2004. Summary of results. Joint NTGS–GA geochronology project: August 2003–December 2003. *Northern Territory Geological Survey, Record* 2004-004. https://geoscience.nt.gov.au/gemis/ntgsjspui/handle/1/82425

Zack T, Stockli DF, Luvizotto GL, Barth MG, Belousova E, Wolfe MR and Hinton RW, 2011. In situ U–Pb rutile dating by LA-ICP-MS: ^{208}Pb correction and prospects for geological applications. *Contributions to Mineralogy and Petrology* 162, 515–530. doi:10.1007/s00410-011-0609-4

APPENDIX 1

Imagery of mineral grains and analysis locations in external attached .tiff and .png files.

APPENDIX 2

LA–ICP–MS U-Pb data in external attached Microsoft Excel files and R script used to process data.